NATIONAL ADVISORY COMMITTEE FOR AERONAUTICS

REPORT 1168

SECONDARY FLOWS AND BOUNDARY-LAYER ACCUMULATIONS IN TURBINE NOZZLES

By HAROLD E. ROHLIK, MILTON G. KOFSKEY, HUBERT W. ALLEN, and HOWARD Z. HERZIG

1954

For sale by the Superintendent of Documents, U. S. Government Printing Office, Washington 25, D. C. Yearly subscription, $10; foreign, $11.25; single copy price varies according to size --------- Price 30 cents

REPORT 1168

SECONDARY FLOWS AND BOUNDARY-LAYER ACCUMULATIONS IN TURBINE NOZZLES

By HAROLD E. ROHLIK, MILTON G. KOFSKEY,
HUBERT W. ALLEN, and HOWARD Z. HERZIG

Lewis Flight Propulsion Laboratory
Cleveland, Ohio

National Advisory Committee for Aeronautics

Headquarters, 1512 H Street NW., Washington 25, D. C.

Created by act of Congress approved March 3, 1915, for the supervision and direction of the scientific study of the problems of flight (U. S. Code, title 50, sec. 151). Its membership was increased from 12 to 15 by act approved March 2, 1929, and to 17 by act approved May 25, 1948. The members are appointed by the President, and serve as such without compensation.

Conduct, under unified control, for all agencies, of scientific research on the fundamental problems of flight

REPORT 1168

SECONDARY FLOWS AND BOUNDARY-LAYER ACCUMULATIONS IN TURBINE NOZZLES [1]

By Harold E. Rohlik, Milton G. Kofskey, Hubert W. Allen, and Howard Z. Herzig

SUMMARY

An investigation of secondary-flow loss patterns originating in three sets of turbine nozzle blade passages was conducted by means of flow-visualization studies and detailed flow measurements. For all cases, high loss values were measured in the fluid downstream of the corners formed by the suction surfaces of the blades and the shrouds, and these losses were accompanied by discharge-angle deviations from design values. Despite the sizes of the loss regions and angle gradients, over-all mass-averaged blade efficiences were of the order of 0.99 and 0.98 and, therefore, are not a good index of blade performance.

This report shows that the inner-wall loss core associated with a blade of a turbine nozzle cascade is largely the accumulation of low-momentum fluids originating elsewhere in the cascade. This accumulation is effected by the secondary-flow mechanism, which acts to transport the low-momentum fluids across the channels on the walls and radially in the blade wakes and boundary layers. At one flow condition investigated, the radial transport of low-momentum fluid in the blade wake and on the suction surface near the trailing edge accounted for approximately 65 percent of the inner-wall loss core, about 30 percent resulting from flow in the thickened boundary layer on the suction surface, and about 35 percent from flow in the blade wake.

The degree to which blade-surface velocity profiles affect the magnitude and concentration of loss cores was investigated by comparing three nozzle blade configurations. Flow-visualization studies and flow measurements at the lower Mach numbers indicate that when, as a result of unfavorable blade-surface velocity profiles, thickened blade boundary layers exist on the blades near the outer shroud, they may provide the conditions required for passage vortex formation. Under these conditions, sizable outer-shroud loss cores are found at the nozzle discharges. Blades having thinner two-dimensional profile boundary layers, however, appear to offer resistance to passage vortex formation near the outer shroud, and, instead, there results inward radial flow of low-momentum air in the blade wake. Under these conditions, the inner-shroud loss region at the nozzle discharge is large, while the outer-shroud loss region may, in comparison, be quite small.

In both cases, reduced loss accumulations along the outer shroud are obtained at the higher Mach number as shock-boundary-layer thickening on the blade surface provides an additional path for the radially inward flow of low-momentum fluid. The results, therefore, indicate that passage vortex formation may not exist for all blade configurations and flow conditions and may be governed, to a large extent, by blade boundary-layer thickness and separation. Comparison of well-designed constant-discharge-angle and free-vortex type blades indicates that the secondary-flow loss differences for these blades are so small that the choice of the type of blading, based solely on secondary flows, is of negligible concern.

INTRODUCTION

Whenever turning of a fluid is accomplished, as by a cascade, a balance is established between static-pressure gradients and centrifugal forces in that fluid. In an annular cascade, where three-dimensional turning is involved, both radial and circumferential static-pressure gradients exist. These pressure gradients, developed in the mainstream, are imposed upon the boundary layers of low-momentum fluid on the walls and on the blades of the cascade. Turning in the boundary layers equal to the free-stream turning would not be sufficient to maintain balance between the pressure gradients and the centrifugal forces. Thus, more than free-stream turning of the low-momentum boundary-layer fluids results. The deviations in flow of the boundary layer from the free-stream flow directions are called secondary flows. Secondary flows inevitably result from the turning of fluids having boundary layers; in annular cascades, a system of three-dimensional secondary flows must always be established.

As gas velocities through turbines are increased to obtain increased power and increased mass flow per unit frontal

[1] Supersedes NACA TN 2871, "Experimental Investigation of Loss in an Annular Cascade of Turbine-Nozzle Blades of Free Vortex Design," by Hubert W. Allen, Milton G. Kofskey, and Richard E. Chamness, 1953; TN 2909, "Study of Secondary-Flow Patterns in an Annular Cascade of Turbine Nozzle Blades with Vortex Design," by Harold E. Rohlik, Hubert W. Allen, and Howard Z. Herzig, 1953; and TN 2989, "Comparison of Secondary Flows and Boundary-Layer Accumulations in Several Turbine Nozzles," by Milton G. Kofskey, Hubert W. Allen, and Howard Z. Herzig, 1953.

area, the three-dimensional secondary flows become increasingly significant, because these secondary flows give rise to relatively large regions of low-energy fluids that cause main-flow blockages and deviations from design flow angles, with consequent reduced efficiency and performance. As transonic velocities are approached, the secondary flows resulting from the radial gradients of pressure, velocity, and circulation become too large to be ignored in the design of turbine blades. Various analytical methods have been developed (refs. 1 to 4) to evaluate and predict the deviations in exit flow angles and velocities due to the secondary flows in flow channels. However, as a result of the complicated three-dimensional patterns of the secondary flows, considerable doubt exists as to whether a physically valid analytical description of secondary flows in turbine nozzle cascades can at present be obtained by use of such simplifying assumptions as two-dimensional flows, no viscosity in the turning fluid, or nontwisting Bernoulli surfaces, which are currently used for theoretical analyses. Accordingly, recent investigations at the NACA Lewis laboratory have concentrated on obtaining experimentally an over-all picture of the actual secondary flows. In reference 5, flow-visualization techniques were employed to trace the boundary-layer flow patterns, and the results were recorded photographically. By these means, the basic patterns of secondary flows and the governing flow parameters in turbomachines were established.

In order to obtain a better understanding of the flow processes within typical modern turbine nozzle blade rows, the series of investigations reported herein was made. Three blade configurations were investigated: blade A, a constant-discharge-angle blade with smooth surface velocity profile designed by the stream-filament method; blade B, a constant-discharge-angle blade with a more blunt leading edge and a more irregular surface velocity distribution with velocity peaks; and blade C, a stream-filament-design blade having free-vortex velocity distribution and a smooth velocity profile. In addition, a series of blade modifications was applied to the blade C nozzle configuration in order to separate and evaluate the various secondary-flow components there. These modifications consisted of blade boundary-layer flow fences and notches cut into the blade trailing edges.

Detailed data were taken, including surveys of total pressure and discharge angle in the free-stream, wake, and boundary-layer regions immediately downstream of the nozzle-discharge sections. Flow-visualization techniques were also employed, including surface flow studies (by means of hydrogen sulfide and paint traces) and smoke flow studies as described in reference 5. The location and direction of the secondary-flow components in the cascades are presented. The angle gradients associated with the secondary-flow systems and their effect on rotor blade angles of attack are also discussed. The blade suction-surface velocity profile is considered, and the degree to which it affects the magnitude, concentration, and location of the high-loss regions is investigated by comparing the three nozzle blade configurations.

These experimental investigations were made by use of the facilities of the NACA Lewis laboratory in 1953.

SYMBOLS

The following symbols are used in this report:

M_H	hub discharge Mach number
P	local total pressure, in. Hg
P_1	reference inlet total pressure, in. Hg
p	local static pressure, in. Hg
r	radius measured from axis, ft
V	local velocity, ft/sec
V_a	local axial component of velocity, ft/sec
V_i	ideal velocity as determined by reference inlet total pressure and local discharge static pressure, ft/sec
V_θ	local tangential component of velocity, ft/sec
x	local measured value, variable used in mass-averaging expression
Γ	circulation, sq ft/sec
γ	ratio of specific heats
η	local blade efficiency, V^2/V_i^2
$d\theta$	increment in circumferential distance
ρ	static density, slugs/cu ft

APPARATUS

TEST UNIT

A schematic view of the test unit used in this investigation is shown in figure 1. A filter was installed in a large depression tank (not shown in the figure) upstream of the test section to prevent damage and clogging of the delicate instruments by dirt particles from the air supply. The filter consisted of two layers of 1/4-inch felt separated by filter paper supported by wire-mesh screening. A second depression tank downstream of the first tank was located approximately 4 duct diameters (approximately 6 ft) upstream of the nozzle blades (fig. 1). A long-radius nozzle was installed in this depression tank to provide smooth entry into the duct leading to the nozzle blades in the test section. A fine mesh screen was also installed in the tank to give a uniform inlet velocity distribution. The air discharged from the nozzle blades into an annular duct having six straightening vanes located approximately 3 tip diameters downstream of the nozzle blades.

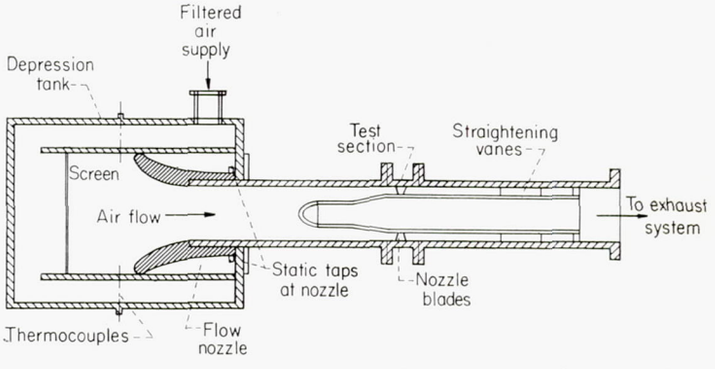

FIGURE 1.—Schematic view of annular-nozzle cascade test unit.

TURBINE NOZZLE BLADES

For simplicity, the three blade configurations investigated will be designated as follows: blade A, a constant-discharge-angle blade with smooth surface velocity profile designed by the stream-filament method; blade B, a constant-discharge-angle blade with a more blunt leading edge and a more irregular surface velocity distribution, particularly

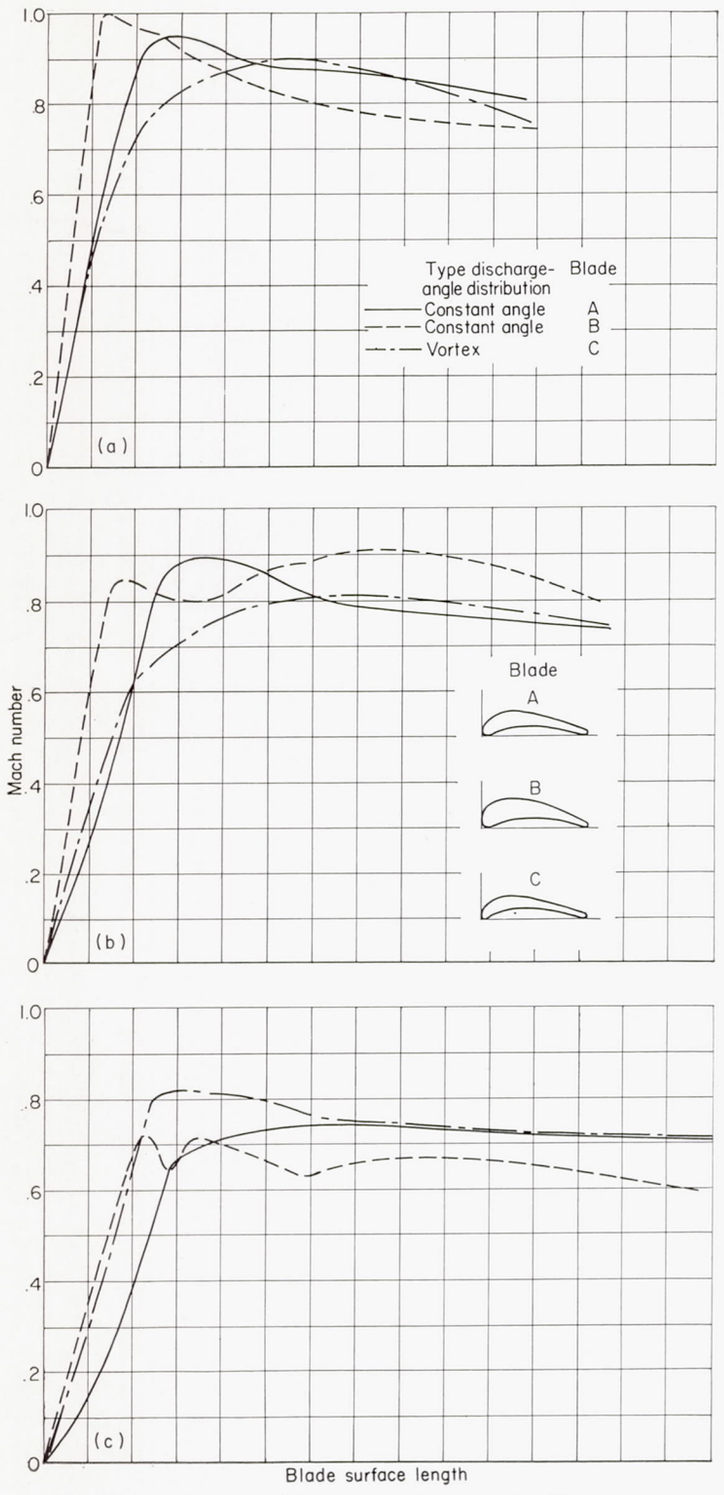

(a) Hub section. (b) Mean section. (c) Tip section.

FIGURE 2.—Design velocities for blade suction surface.

near the blade tip; and blade C, a stream-filament-design blade having free-vortex velocity distribution and a smooth velocity profile. The suction-surface velocity profiles at the hub, mean, and tip sections of the three blades are presented in figure 2. Mean-section blade shapes are shown in figure 2 (b).

All nozzle blades used in the investigation were of subsonic design for an equivalent weight flow of approximately 15.3 pounds of air per second. Each set consists of 48 blades having a hub-tip radius ratio of 0.730 and a tip diameter of 16.25 inches. Blades A and C were designed by the two-dimensional stream-filament method described in reference 6. As the stream-filament method applies only to the portion of the blades forming the channel, the blades were designed to do the greatest amount of the turning within the channel. The trailing-edge portions of the blades, having little curvature, were faired at the approximate discharge angle. Blade profile and stacking coordinates for the three blade sets are given in tables I to III.

Constant-discharge-angle blades (blade A).—These blades were designed for a constant discharge angle of 56° from axial. The blade chord varies from 1.642 inches at the tip to 1.173 inches at the hub, while the trailing-edge thickness varies from 0.049 to 0.034 inch. The blades have a solidity of 1.510 at the hub and 1.545 at the tip.

Constant-discharge-angle blades (blade B).—These blades, from a production turbine, were designed for a constant discharge angle of approximately 60° from axial and have a solidity of 1.489 at the hub and 1.497 at the tip. The chord varies from 1.592 inches at the tip to 1.157 inches at the hub, and the trailing-edge thickness from 0.040 to 0.026 inch.

Vortex-type blades (blade C).—These blades were designed for a free-vortex-type velocity distribution with a discharge angle of approximately 65° from axial at the hub. The blades have a solidity of 1.507 at the hub and 1.595 at the tip. The chord and trailing-edge thickness vary from 1.696 and 0.044 inch, respectively, at the tip to 1.172 and 0.034 inch at the hub.

Modified vortex-type blades (modified blade C).—The modifications shown in figure 3 were adopted in the attempt to separate and evaluate the various components of secondary flow. These are:

(1) The full flow fence (fig. 3 (a)) at blade mean radius for interrupting radial flows in the wake of the blade and on the suction surface near the trailing edge

(2) The modified flow fence for interrupting radial flows in the wake, but not in the thickened boundary layer on the suction surface of the blade near the trailing edge (fig. 3 (b))

(3) A $\frac{3}{16}$-inch notch in the blade trailing edge (fig. 3 (c))

(4) A $\frac{3}{8}$-inch notch in the blade trailing edge (fig. 3 (d))

INSTRUMENTATION

The cascade was instrumented to obtain surveys of total and static pressures at the inlet measuring station 0.5 inch upstream of the leading edge of the tip section of the blades. Total pressures, wall static pressures, and flow angles were surveyed at the discharge measuring station 0.159 inch downstream of the trailing edge of the nozzle blade tip. The instruments used to obtain the detailed surveys of the gas state at the inlet and discharge are shown in figure 4.

Total-pressure probes.—Two types of total-pressure probe were used to measure total pressure at the discharge measuring station. One type was designed specifically for measurements in the boundary layer; the other, for free-stream measurements. The pressure-measuring head of the boundary-layer probe (fig. 4 (a)) consisted of 0.015-inch-outside-diameter tubing. The tip was flattened to approxi-

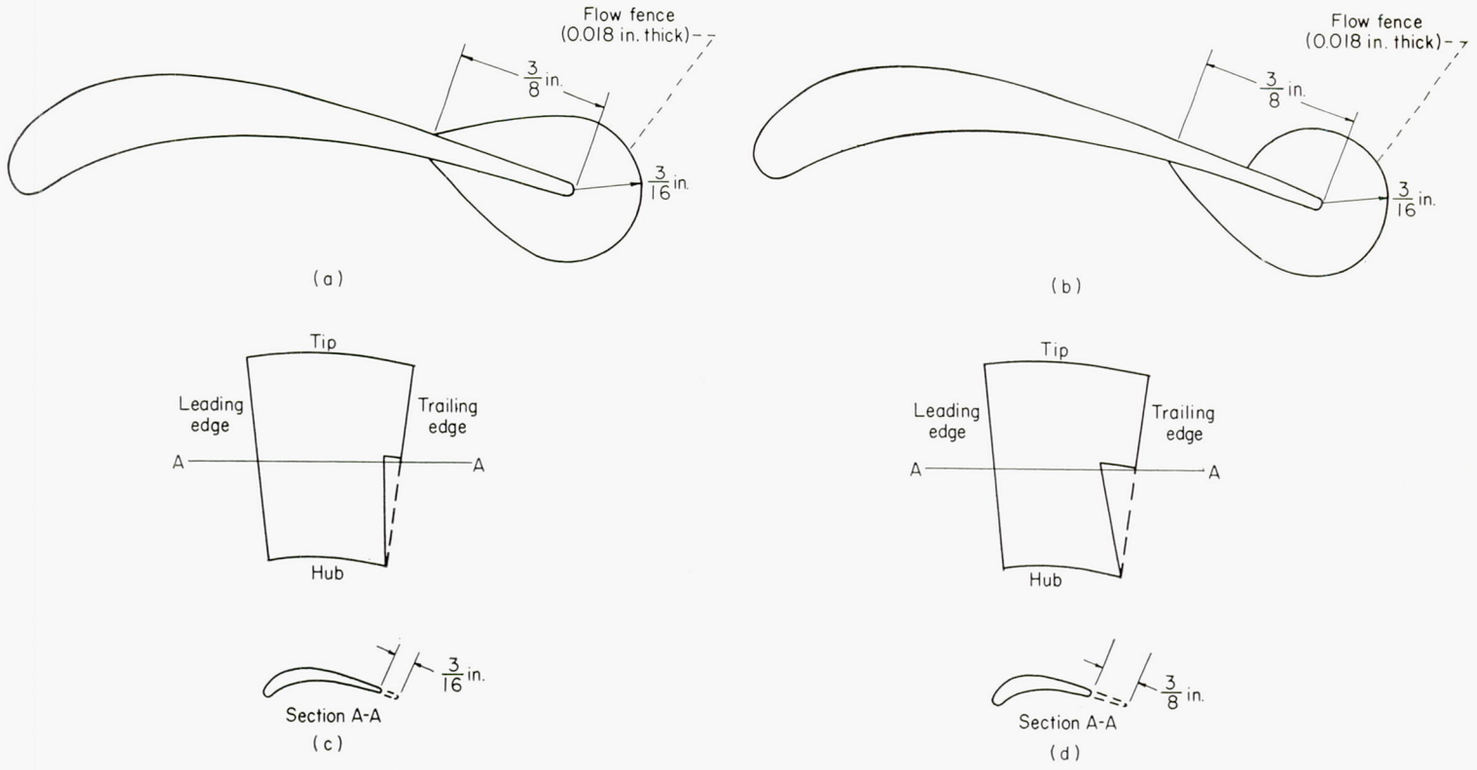

(a) Full flow fence.
(c) 3/16-Inch notch.

(b) Reduced flow fence.
(d) 3/8-Inch notch.

FIGURE 3.—Sketches of various modifications.

mately 0.003-inch inside minor axis length (parallel to probe axis) to obtain closer approximations of point values in the regions of high radial pressure gradients. The three-dimensional total-pressure probe (fig. 4 (b)) was designed to measure the total pressure outside the boundary layer for radial flow angles within the limits of approximately $\pm 9°$. The probe consists of five 0.015-inch-outside-diameter tubes projecting 0.120 inch from the probe axis. The tubes were set at angles of 3°, 6°, −3°, −6°, and 0° from a plane normal to the axis of the probe and with the measuring ends of the tubes in this plane. A shielded total-pressure probe was used to measure the reference total pressure at the inlet to the blades.

Static-pressure taps.—Wall static taps of 0.015-inch diameter were located at both the inner and outer shroud in the inlet and discharge measuring planes. At the inlet measuring plane, one static tap each at the inner and outer shrouds was located at the circumferential position used for the inlet radial surveys. At the discharge measuring plane, static pressures were measured by eight closely spaced static-pressure taps in either wall.

Flow-angle measuring probes.—A double-wire hot-wire-anemometer probe (fig. 4 (c)) was used to measure the discharge flow angles in the mainstream. The instrument consists of two parallel wires supported by two prongs and mounted under tension on the axis of the probe (parallel to a radius of the cascade). Thus, the wires can be rotated without appreciable displacement. Each of the wires has a diameter of approximately 0.0009 inch and a length of 0.045 inch or less. The distance between wire centers is 0.005 inch.

For use in the inner-shroud boundary layer, a V-wire hot-wire anemometer (fig. 4 (d)) was constructed, having the two wires mounted in such a way that both were in the same plane and parallel to the shroud surface (perpendicular to a radius of the cascade) when in use. The wires of this instrument were 0.0011 inch in diameter and 0.050 inch long. They were mounted on three supports, the tips of which were located at the corners of an equilateral triangle. Thus, the two wires mounted near the support tips formed a V with a 60° angle at their intersection. The use of such an instrument near the inner shroud was based on the assumption that no steep circumferential gradients of angle or mass flow would be present. Details of design of wire supports and the general construction of the hot-wire probes are discussed in reference 7. The application of hot-wire-anemometer probes to the measurement of discharge flow angles for the flow conditions reported in this investigation is discussed in the appendix.

A double-tube pressure probe (fig. 4 (e)) also was used for angle measurements in the boundary layer. In order to minimize effects of pressure gradients and angle gradients on the measured angles, the tube dimensions were made small. Each tube was of 0.010-inch-outside-diameter stainless steel. The tubes were soldered together and mounted in such a way that the double open end had its axis lying in a circumferential plane and could be rotated about a radial axis. In order to increase the sensitivity to

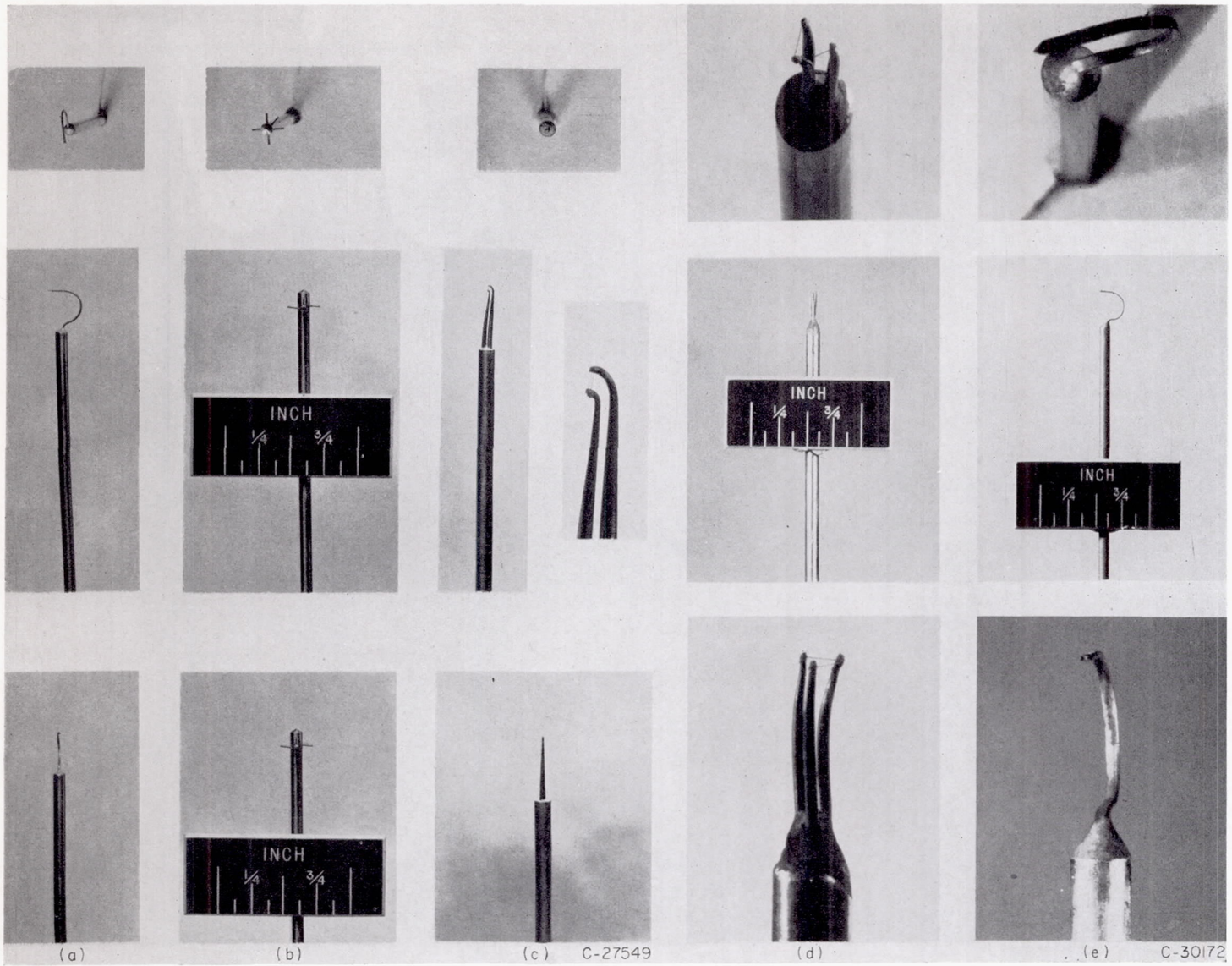

(a) Boundary-layer probe.

(b) Three-dimensional total-pressure probe.

(c) Parallel-wire anemometer probe.

(d) V-wire anemometer probe.

(e) Double-tube angle probe.

FIGURE 4.—Survey instruments.

flow direction, each tube end was ground back at an angle of 30° from the soldered tip junction so that the tip was wedge-shaped with a 60° total angle.

Repeatability.—Discharge total pressures in the free stream, wakes, and boundary layers, and wall static pressures could be repeated within ±0.05 inch of mercury during any extended time interval. The reproducibility of ±0.05 inch was maintained by observing the data when the reference static pressure was steady at the desired set value.

The flow-angle measurements made with any given probe could be repeated within ±0.5° with that probe. At the lower Mach number, the two boundary-layer angle probes gave data that resulted in contour lines of approximately the same shape. Maximums and minimums were in the same positions and had the same magnitudes to about ±1.0°. V-wire data from the boundary layer could be faired into parallel-wire data from the main part of the annulus with adjustments of not more than about ±1.0°.

Agreement between probes was not so close at the higher Mach number because of the higher gradients in angle and mass flow encountered. The effects of these gradients are different for each type of probe. The two boundary-layer probes showed angle gradients in the same direction over much of the region where they were used, but the magnitudes of the gradients did not agree. However, at this Mach number the pressure-probe angle data were in moderately good agreement with parallel-wire data in the region where the data overlapped. Therefore, pressure-probe angle data were used to make contours between points 0.005 and 0.080 inch from the inner shroud, and parallel-wire data were used

between the outer shroud and points 0.120 inch from the inner shroud. Contours were then faired in between 0.080 and 0.120 inch from the inner shroud.

PROCEDURES

The series of investigations reported herein began chronologically with blade B, followed by the investigations of blade C, modified blade C, and finally blade A. New and improved instrumentation and flow-study techniques were developed during the course of the protracted investigation and were applied to all succeeding blade studies as rapidly as they were perfected. So it is that the studies of surface flow direction were first made on blade C. Likewise, the double-tube pressure probe for boundary-layer flow-angle surveys was not perfected until near the end of the investigation of blade C and the blade C modifications and, therefore, was not used extensively until the blade A investigation.

EXPERIMENTAL PROCEDURE

In general, the flow measurements and flow-visualization studies of blades B and A were made similarly to those of blade C. At the time of the investigation of blade B, which was conducted first, the techniques required for boundary-layer and surface flow studies had not yet been developed; therefore, these studies were not made for blade B.

Flow conditions.—The reference inlet total pressure was held constant at approximately 26.50 inches of mercury absolute, and the inlet total temperature at 553° R for all surveys. Each of the three sets of blades was investigated at two hub discharge Mach numbers as follows: blade A, 0.86 and 1.36; blade B, 1.18 and 1.41; blade C, 0.94 and 1.46. Smoke studies of flow direction were made on blades A and B at very low air velocities.

Inlet surveys.—Radial surveys of total pressure and static pressure were made at only one circumferential location at the inlet, because preliminary surveys indicated little measurable circumferential variation in either total or static pressure. One static tap each on the inner and outer shrouds furnished the static-pressure values for the end points. Preliminary angle surveys indicated little variation from the axial direction over the blade passage, and the inlet velocity distribution was therefore satisfactory for the investigation.

Discharge static pressure.—Wall static-pressure values for the nozzle discharge were obtained from the static taps located in the discharge measuring plane. For purposes of velocity calculations, static pressure was assumed to vary linearly from inner to outer shroud.

Discharge total-pressure surveys.—At the discharge measuring station, circumferential surveys of total pressure were made covering an arc corresponding to one complete passage with some overlap. These surveys were spaced radially in such a way as to cover boundary layers and loss regions in detail and at the same time to survey other regions closely enough to verify the existence of uniform flow. Circumferential points were likewise spaced to give detailed information in loss regions and wakes. Determination of the radial position of the probe within 0.002 inch in the annulus behind the blades was required in order to locate accurately the wakes, boundary layers, and loss regions with respect to the walls. For this reason, the inner shroud as a reference position was located by use of a low-voltage electric circuit that indicated by a light when contact was made between the measuring probe and the inner shroud.

Free-stream total pressures were measured with the five-tube total-pressure probe. Each of the five tubes was rotated into the stream for a maximum reading, and the greatest total-pressure reading obtained from the readings of the five tubes was taken as the total-pressure value for the survey point.

Discharge-angle surveys.—Surveys of discharge angle were made covering the same blade passage as was covered with the total-pressure surveys. In the free-stream part of the annulus, where it was assumed that high angle gradients or mass-flow gradients, if any, would be largely circumferential (as in the blade wake) rather than radial, the parallel-wire anemometer was considered applicable. In the shroud boundary layers, where it was assumed that such gradients would be largely radial rather than circumferential, the V-wire anemometer is more suitable. Actually, the parallel-wire instrument performed well wherever used, and measurements were made with it from the outer shroud to points 0.1 inch from the inner shroud. Near the outer shroud it served to confirm the existence of a steep radial angle gradient; but since the area involved in this loss region was comparatively small, it was given no further attention, although the accuracy might have been improved by use of the V-wire probe.

Near the inner shroud the parallel-wire probe could not be used, not only because of diminished accuracy but also because the distance between survey point (considered as the wire center) and surface was limited to about 0.035 inch. Therefore, data were taken with the V-wire anemometer in the region within 0.2 inch of the inner shroud. These data were satisfactory at the lower Mach numbers; but, at the higher Mach numbers, circumferential gradients of angle and mass flow were sufficient to require the use in this region of the double-tube pressure probe, the results from which would be less susceptible to the effects of such gradients.

The use of the double-tube pressure probe for boundary-layer flow-angle surveys was developed near the end of the investigation of blade C. In the investigation of blade A, a comparison was made of the free-stream angles measured by the double-wire hot-wire-anemometer probe and the double-tube pressure probe. Differences in measured angles were found to be 1° or less over most of the passage. The greatest difference, approximately 2°, occurred near the shrouds where the rates of radial variation in discharge angle were large. Because of its small size, the double-tube pressure probe is considered more reliable than the double-wire hot-wire-anemometer probe in regions where the rate of radial variation in discharge angle is high. Because of this and because of its greater simplicity in operation, all angle data in the free stream and in the boundary layers (for blade A) were taken with the double-tube pressure probe. No flow-angle measurements were made at positions less than 0.1 inch from the shrouds for blade B.

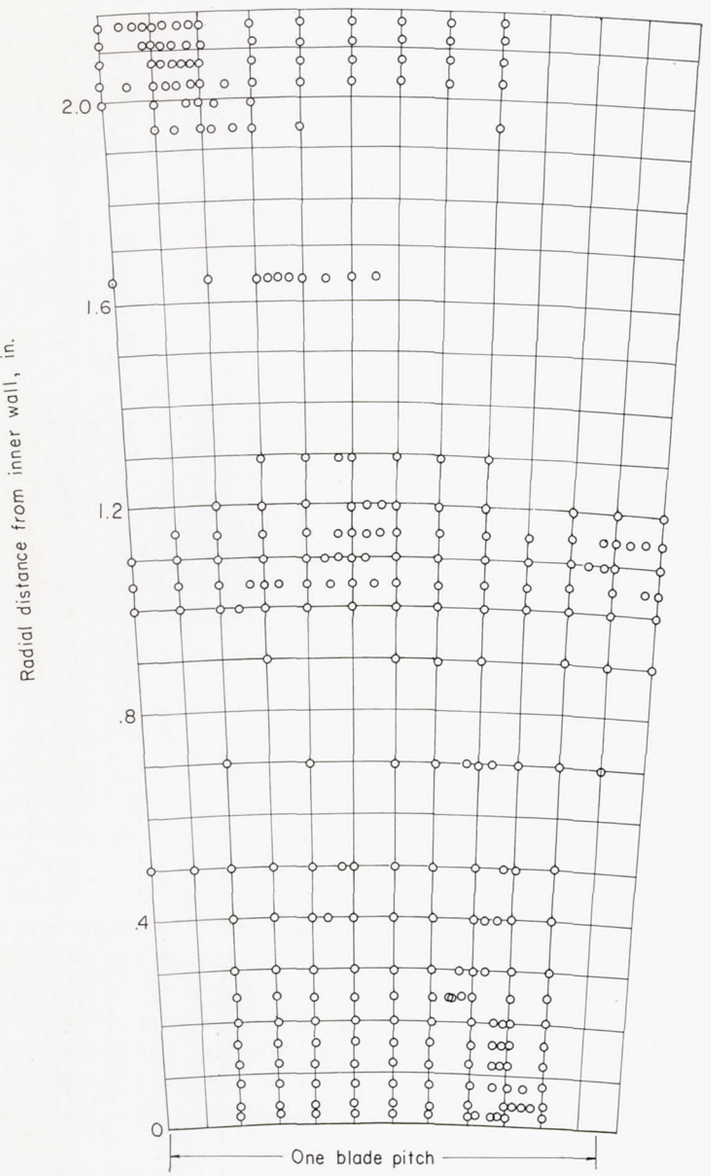

FIGURE 5.—Total-pressure measurement points for full-flow-fence modification (fig. 3 (a)). Hub Mach number, 1.46.

Blade C modification studies.—Effects of the various modifications on loss distribution in the measuring plane for blade C were investigated at the same two hub discharge Mach numbers as for the unmodified blade C, that is, 0.94 and 1.46. Circumferential surveys of total pressure were made at several radial positions in the measuring plane. These surveys, as well as points in each survey path, were spaced to give a detailed picture of each loss region. This spacing varied from one modification to the next because of the differences in loss distribution. An example of the distribution of survey points is shown in figure 5, where the locations of the total-pressure measurement points are plotted for the full-flow-fence modification at the higher Mach number.

Static-pressure values for points in the stream were calculated from pressure measurements made with wall static taps. It was assumed in this calculation that the static pressure varied linearly from inner to outer wall along lines in the radial measuring plane which were approximately parallel to the blade wakes.

Surface flow-direction studies.—Visual studies of the flow direction along the blade and wall surfaces for blades A and C were made in two ways (ref. 5). The first technique used the reaction between white lead carbonate painted on the surface and hydrogen sulfide gas admitted through an appropriately located wall static tap and mixed with the boundary-layer air flowing through the cascade. The resulting darkening of the lead carbonate showed the direction of flow along the surface from the static tap. The hydrogen sulfide gas pressure was adjusted to exceed the static pressure at the tap by only enough (0.02 in. Hg, approximately) to cause it to flow into the passage without blowing it away from the surface and without upsetting local flow conditions. The second technique involved softening the lead carbonate with glycerin until it would flow slightly along the surface because of viscous effects between air and paint. A comparison of results obtained by these two techniques showed good agreement; hence, patterns on the surface were considered to indicate air-flow direction, and the results were recorded photographically.

Smoke flow-direction studies.—Smoke studies of flow direction using the technique of reference 5 were made with blade types A and B mounted in the annular cascade (fig. 1). The airspeed through the cascade was held to a maximum of about 20 feet per second in order to avoid diffusion of the smoke and keep the smoke sufficiently concentrated for photographing. The smoke was introduced into the air stream just upstream of the blades at two radial positions for each blade, namely, adjacent to the outer shroud and near midsection. Photographs were made of the resulting flow patterns at the blade discharge.

CALCULATION PROCEDURE

Loss calculations.—Results of total- and static-pressure-tap data are presented as contours of kinetic-energy loss, which is defined as follows:

$$\text{Loss}=1-\eta=1-\frac{V^2}{V_i^2}=\frac{\left(\frac{p}{P}\right)^{\frac{\gamma-1}{\gamma}}-\left(\frac{p}{P_1}\right)^{\frac{\gamma-1}{\gamma}}}{1-\left(\frac{p}{P_1}\right)^{\frac{\gamma-1}{\gamma}}}$$

The error involved in the losses calculated from pressure measurements made at the lower hub discharge Mach numbers is believed to be negligible. At the higher hub discharge Mach numbers, however, the total pressures indicated by the probes are low because of the shock losses associated with the probes. These shock losses varied with position in the measuring plane because of the variation in Mach number and the proximity to the loss regions. Near the hub boundary layer, for example, interaction of the shock wave induced by the probe and the shroud boundary layer produced a thickened boundary layer that influenced flow just upstream of the probe by causing a series of very weak oblique shocks. This boundary-layer thickening upstream of the incident shock wave is discussed in reference 8, which includes schlieren photographs at several shock strengths and Reynolds numbers. Because the air had thus decelerated through a series of weak oblique shocks rather than one nor-

mal shock upstream of the probe, the indicated total pressure was higher than that considered possible for the Mach number level and a normal shock. Therefore, accurate correction for the error induced by the presence of the probes at each measuring point in the stream is extremely difficult.

The static pressures in the stream when the probes were withdrawn indicated that the maximum normal-shock-loss correction necessary anywhere in the measuring plane was slightly greater than 5 percent. The 5-percent loss contours define clearly the loss regions existent with each modification at the higher Mach number and separate the viscous-loss areas from those where this variable probe loss is the only loss. In evaluating the effects of the modifications, then, only the areas within the 5-percent loss contours were considered; this was done simply by assuming that all losses of 5 percent or less were equal to zero.

Mass-averaging.—Discharge angles, velocities, and loss were mass-averaged by the following expression:

$$\frac{\int x\rho V_a \mathrm{d}\theta}{\int \rho V_a \mathrm{d}\theta}$$

The use of weighted averages where possible, in preference to ordinary arithmetic averages, is discussed in reference 9.

Circulation.—Circulation was determined by the following equation:

$$\Gamma = V_\theta r$$

This equation was adapted for use in this investigation from a similar equation developed in reference 10 (pp. 62ff).

RESULTS

INLET SURVEYS

Inlet surveys of total and static pressure and flow angle were practically identical for all three blade configurations. The results of the inlet radial survey of total pressure are plotted in figure 6. Constant total pressure was obtained over most of the flow passage, the losses in total pressure occurring in the wall boundary layers at the blade inner and outer shrouds. As noted earlier, preliminary angle surveys indicated little variation from the axial direction over the blade passage. The combination of constant total pressure,

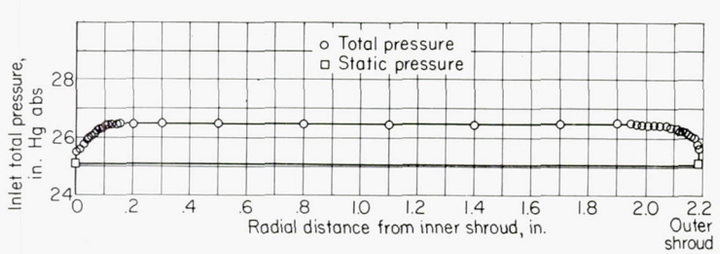

FIGURE 6.—Inlet pressure distribution.

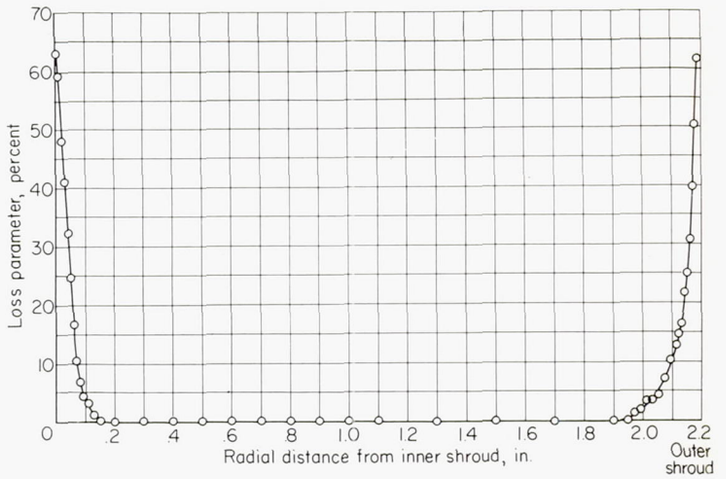

FIGURE 7.—Inlet loss distribution.

static pressure, and flow angle produced an inlet velocity distribution that was considered satisfactory. The radial distribution of inlet loss parameter is shown in figure 7.

DISCHARGE LOSS DISTRIBUTIONS

Results presented include kinetic-energy loss distribution (figs. 8 to 10) and discharge-angle distribution (fig. 11) for the flow investigations of all the blade configurations. Also presented are comparisons of circulation distribution and results of hydrogen sulfide and paint traces and of smoke flow studies. The most extensive tests were made on blade C and blade C modifications. The other configurations, for the purposes of this report, were investigated mainly to enable comparisons with blade C. Accordingly, the results obtained for blade C are presented first and in greatest detail. The presentation of the results obtained with the other configurations is only as complete as is deemed necessary to point up the differences and similarities in the behavior of the various configurations.

Discharge loss for blade C.—At the discharge measuring station of blade C, the Mach numbers were 0.94 and 1.46 adjacent to the inner-shroud boundary layer and 0.75 and 1.06 adjacent to the outer-shroud boundary layer. Results of the total-pressure surveys and static-pressure-tap data are presented in figures 8 (e) and (f) as contours of energy loss. It is to be noted that circumferential coordinate values are plotted differently in the two figures in order to show a complete blade wake as a unit. Figure 8 (f) is a composite of measurements made in different parts of two adjacent wakes.

Negligible losses were obtained over most of the flow passage. The major losses were observed in the shroud boundary layers, in the blade wake, and particularly along the junctions of the shroud boundary layers and the blade wake. The losses in the blade wake were small compared

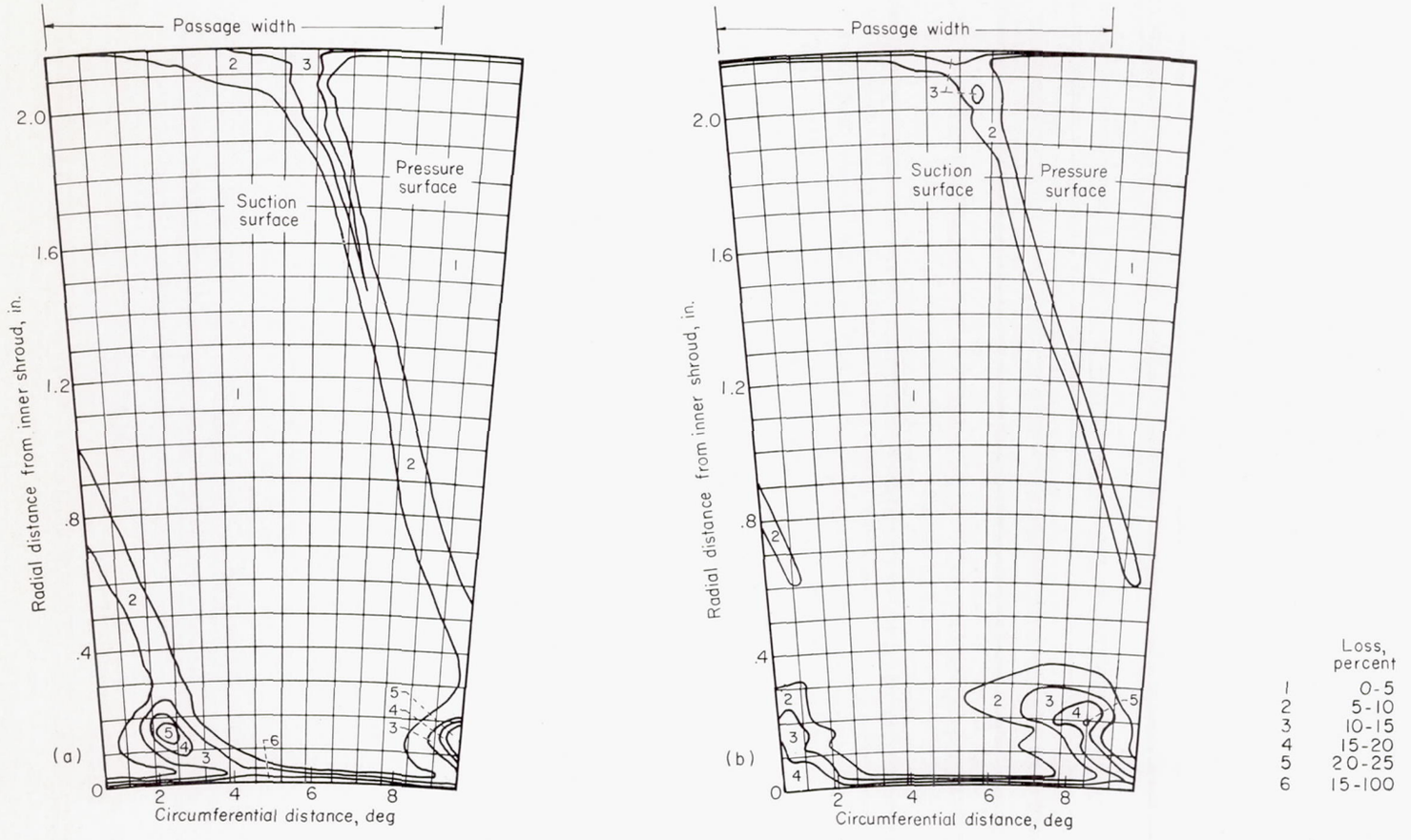

(a) Blade A; lower Mach number (0.86).

(b) Blade A; higher Mach number (1.36).

Figure 8.—Contours of loss across one blade passage.

with those measured in the other loss regions and shroud boundary layers. Maximum losses occurring were 16.2 and 14.3 percent at the inner and outer shroud, respectively, for the lower Mach number run, and 25.2 and 5.3 percent, respectively, for the higher Mach number run. The results show a decrease in loss at the outer shroud with increased Mach number and an increase in loss at the inner shroud with increased Mach number. The changes in the loss picture with Mach number at any radial position are shown in figure 10 (a), for which a loss parameter was mass-averaged circumferentially across a blade passage and plotted against radius.

The data taken in this investigation were used to obtain blade efficiencies. Mass-averaged blade efficiencies were 0.99 and 0.98. Although the mass-averaged blade efficiencies are high, they are not a good index of blade performance. Accumulation of the losses at the junction of the blade and inner shroud, where the velocity gradients are great, could make the flow unstable and induce additional viscous losses and angle gradients.

Discharge loss for blade C modifications.—The results of the total-pressure surveys and static-pressure-tap data for blade C modifications are presented in figure 9. Only the full flow fence was used for the lower Mach number (hub discharge Mach number, 0.94; fig. 9 (a)), because it was found that the blade C modifications were ineffective at this flow condition. All four modifications were tested at the higher flow Mach number, and the results are presented as contours of energy loss in figures 9 (b) to (e). The changes in the loss picture with the flow-fence modifications are shown in figures 10 (b) and (c), in which the loss parameter was mass-averaged circumferentially across a blade passage and plotted against radius.

Discharge loss for blade A.—Negligible losses were observed for blade A over most of the flow passage (figs. 8 (a) and (b)). The major losses were found in the shroud boundary layers, the blade wakes, and particularly in the vicinity of the corners formed by blade suction surfaces and shrouds. The measured blade-wake loss values were small compared with those in the shroud boundary layers and the other loss regions. For the loss regions outside the shroud boundary layers (i.e., more than approximately 0.040 in.

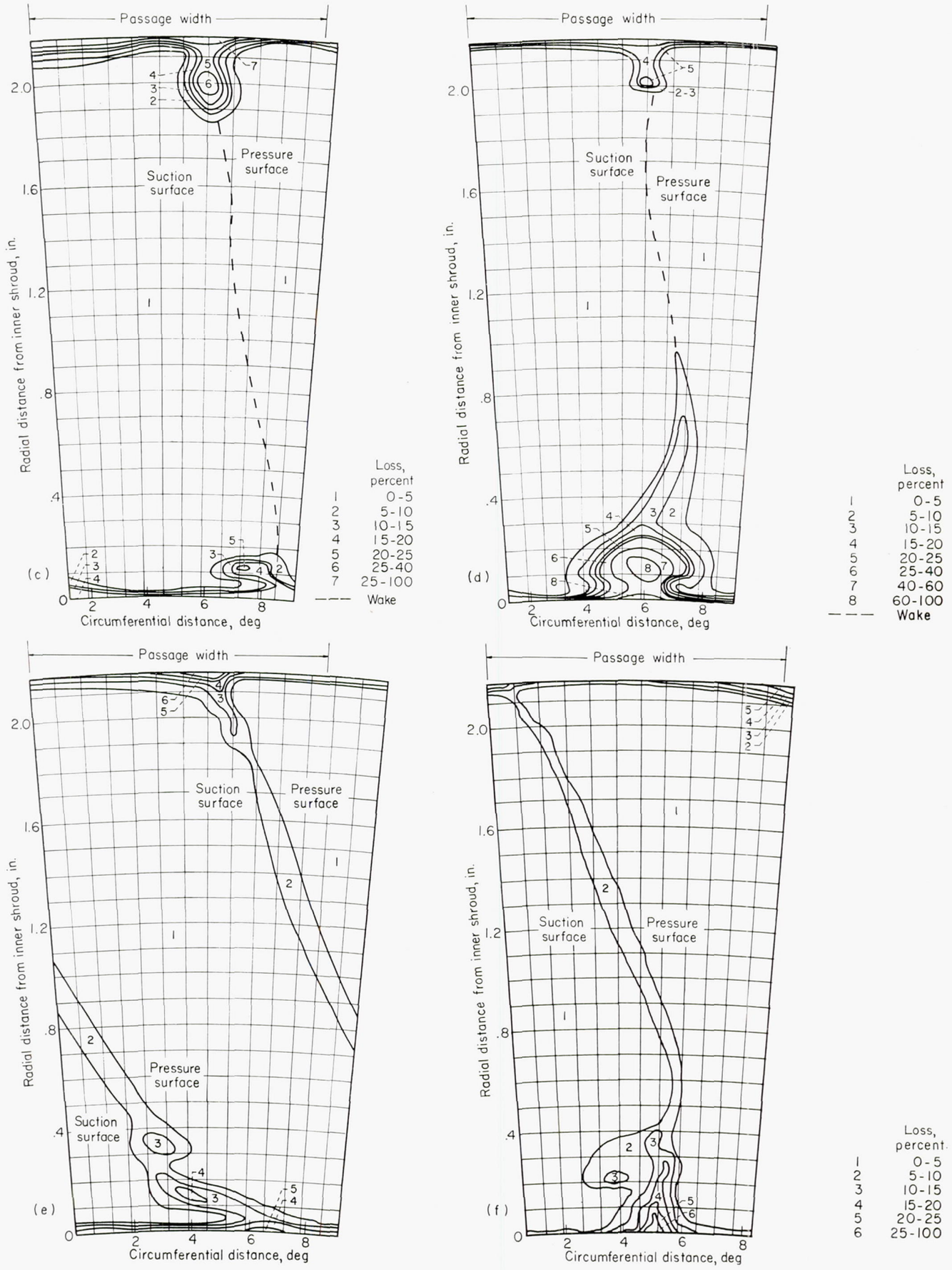

(c) Blade B; lower Mach number (1.18).
(d) Blade B; higher Mach number (1.41).
(e) Blade C; lower Mach number (0.94).
(f) Blade C; higher Mach number (1.46).

FIGURE 8.—Concluded. Contours of loss across one blade passage.

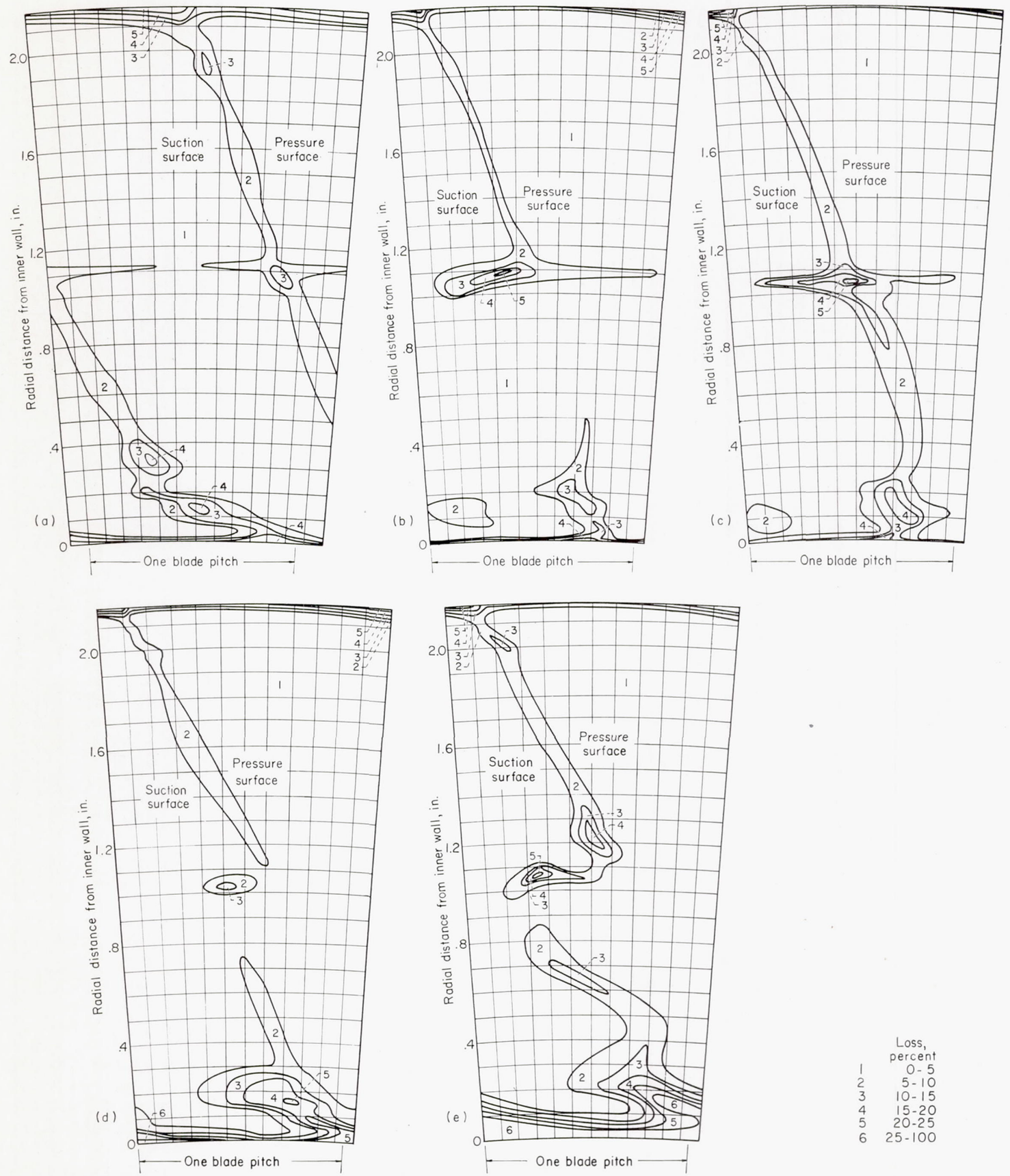

(a) Lower Mach number (0.94); full flow fence. (b) Higher Mach number (1.46); full flow fence. (c) Higher Mach number (1.46); reduced flow fence.
(d) Higher Mach number (1.46); 3/16-inch notch. (e) Higher Mach number (1.46); 3/8-inch notch.

FIGURE 9.—Contours of loss across one blade C passage with blade modifications.

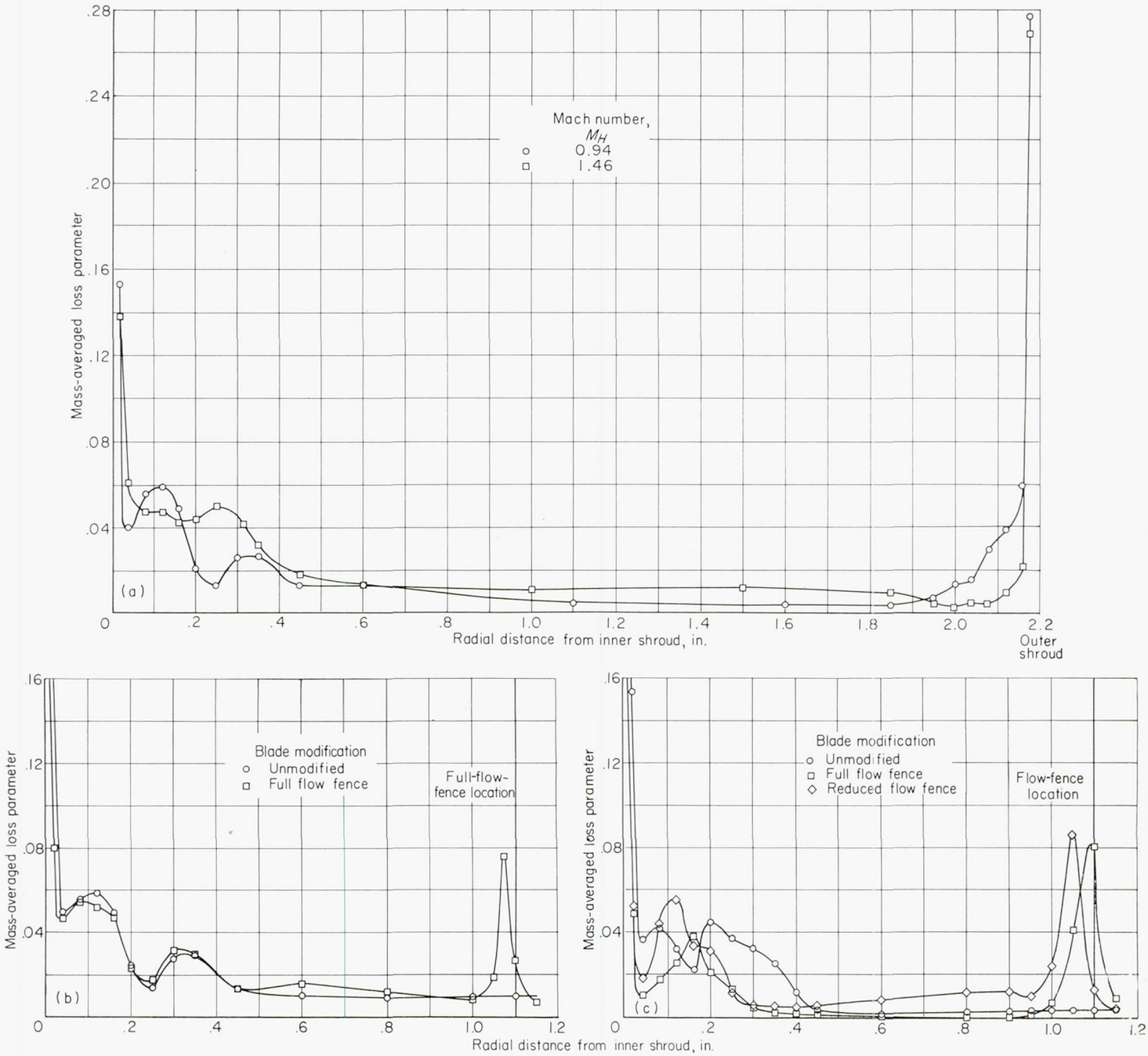

(a) Blade C.

(b) Blade C. Mach number, 0.94; full-flow-fence modification. (c) Blade C. Mach number, 1.46; both flow-fence modifications.

FIGURE 10.—Radial distribution of loss at nozzle discharge.

from the shrouds), loss areas and magnitudes were such as to indicate a reduction in loss near the outer shroud with increasing Mach number and an increase in loss near the inner shroud with increasing Mach number. This result is also shown in the curves of loss plotted against radial position (fig. 10 (d)), where the value at each radial position is obtained by mass-averaging the loss across one passage width at that radius.

Comparison of discharge losses (blades A and C).—No significant difference in magnitude is noted between losses for blades A and C (figs. 8 (a), (b), (e), and (f)). For each blade the size of the loss region and the over-all magnitude of the losses decreased at the outer shroud with increasing Mach number while increasing at the inner shroud. In both cases, the extents of the measured wakes decreased with increasing Mach number (for blade A at the higher Mach number, the wake loss dropped below the 5-percent contour to a minimum of 3.5 percent), but the losses distributed throughout the passage (regions marked 1 on the contour plots) increased with increasing Mach number. This is also apparent in the mass-average plots (figs. 10 (e) and (f)), where the values are affected not only by losses in the boundary layers, loss regions, and wakes but also by losses distributed throughout the passage.

Comparison of discharge losses (blades A, B, and C).—Figures 8 (c) and (d) show loss contours for blade B. Comparison with the contours for blades A and C (figs. 8 (a), (b), (e), and (f)) shows significant differences. At both Mach numbers, the wake loss is small for blade B, being less than 5 percent along almost the entire wake length for the lower Mach number. The outer-shroud loss region for blade B at the lower Mach number is greater in magnitude and extent than that for the other two blades and differs in shape. Although it diminishes with increasing Mach number as for the other blades, it is still appreciable at the higher Mach number. The inner-shroud loss region outside the shroud boundary layer increases with increasing Mach number for blade B as for the other two blades, but for blade B it becomes much larger, maximum loss at the higher Mach number being 67 percent compared with 21 percent for blade A and 25 percent for blade C.

Some of the results indicated by the contour plots also appear on the mass-averaged loss plots (fig. 10). The decrease of the loss at the outer shroud and increase at the inner shroud with increasing Mach number are apparent on the mass-average plots. Also, the difference in flow behavior between blade B and the other two blades shows up as differences between losses in the wakes and near the inner and outer shrouds.

DISCHARGE-ANGLE DISTRIBUTIONS

Discharge angles for blade C.—The results of the discharge-angle surveys are shown as contours in figure 11. Angle gradients for the lower Mach number (fig. 11 (e)) were comparatively small; however, the angle gradients increased with increasing Mach number. The variation in discharge angle across the passage at a radial distance of 0.2 inch from the inner shroud increased from 3.5° for the lower Mach number to 13.6° for the higher Mach number. At the higher Mach number (fig. 11 (f)) the greatest variation in discharge angle occurred in the corner of the passage bounded by the pressure side of the wake and the inner shroud.

In order to determine the effect of the angle variation, calculations of rotor blade angles of attack were made for the higher Mach number where the circumferential angle variations were the greatest. For these calculations, a tip speed of 640 feet per second was assumed. Discharge-flow-angle variations of 13.6°, 5.4°, and 4.0° at radial distances from the inner shroud of 0.2, 1.0, and 2.0 inches, respectively, led to local variations in the rotor blade angle of attack of 16.9°, 6.6°, and 11.3°. An effect of this variation, as discussed in reference 11, was a loss (calculated at a radial position 0.2 in. from the inner shroud) of 1.5 percent of the energy based on tangential component of velocity. Further losses of significant magnitude may also exist because of the effect on the rotor of the pulsating flow caused by variations in nozzle discharge angle.

In figure 12 (a) the circumferential average of discharge flow angle is plotted against radius for each of the two Mach numbers. The measured angles show that in the central part of the passage the turning had approximately design value, but that as either wall was approached there appeared a decrease in discharge angle relative to design value. Near

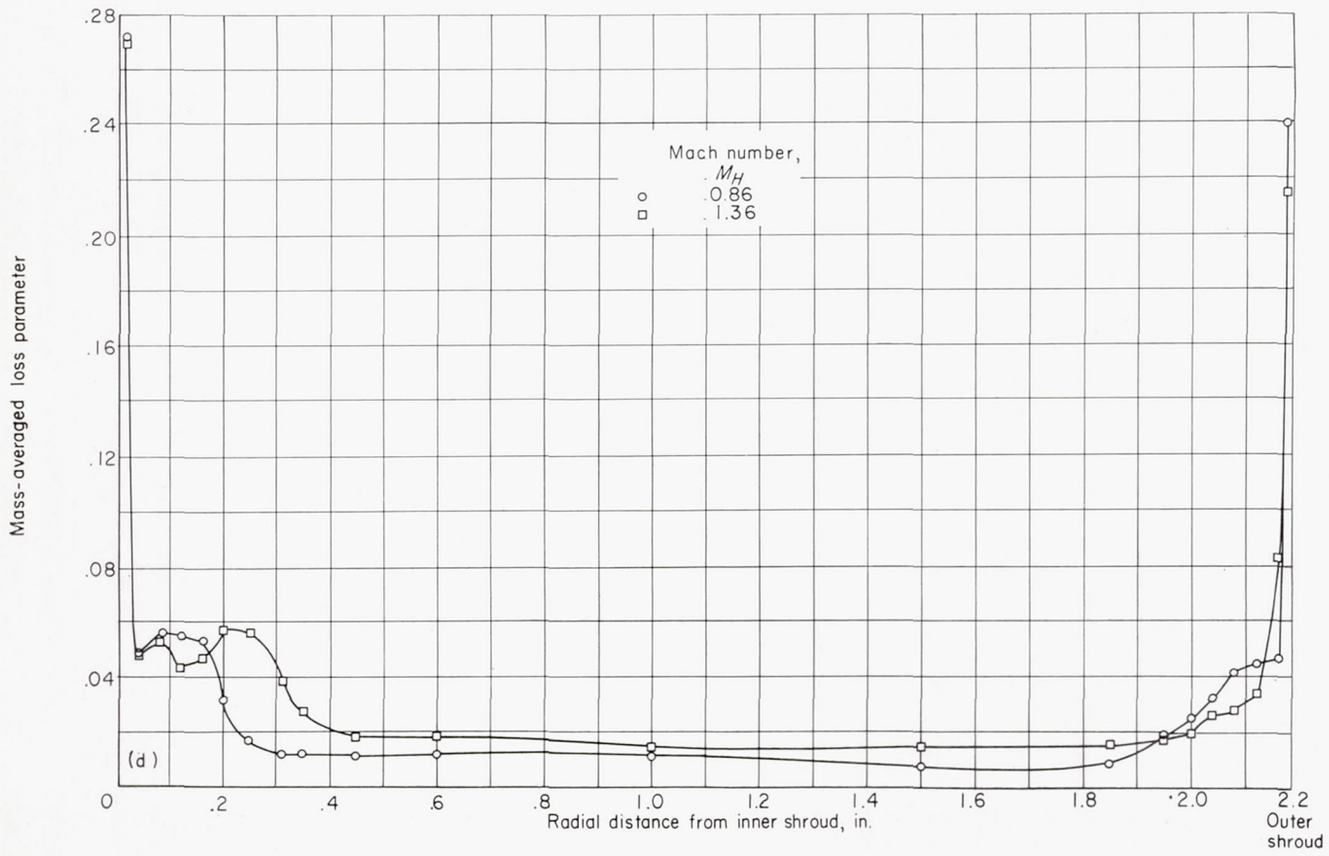

(d) Blade A.

Figure 10.—Continued. Radial distributon of loss at nozzle discharge.

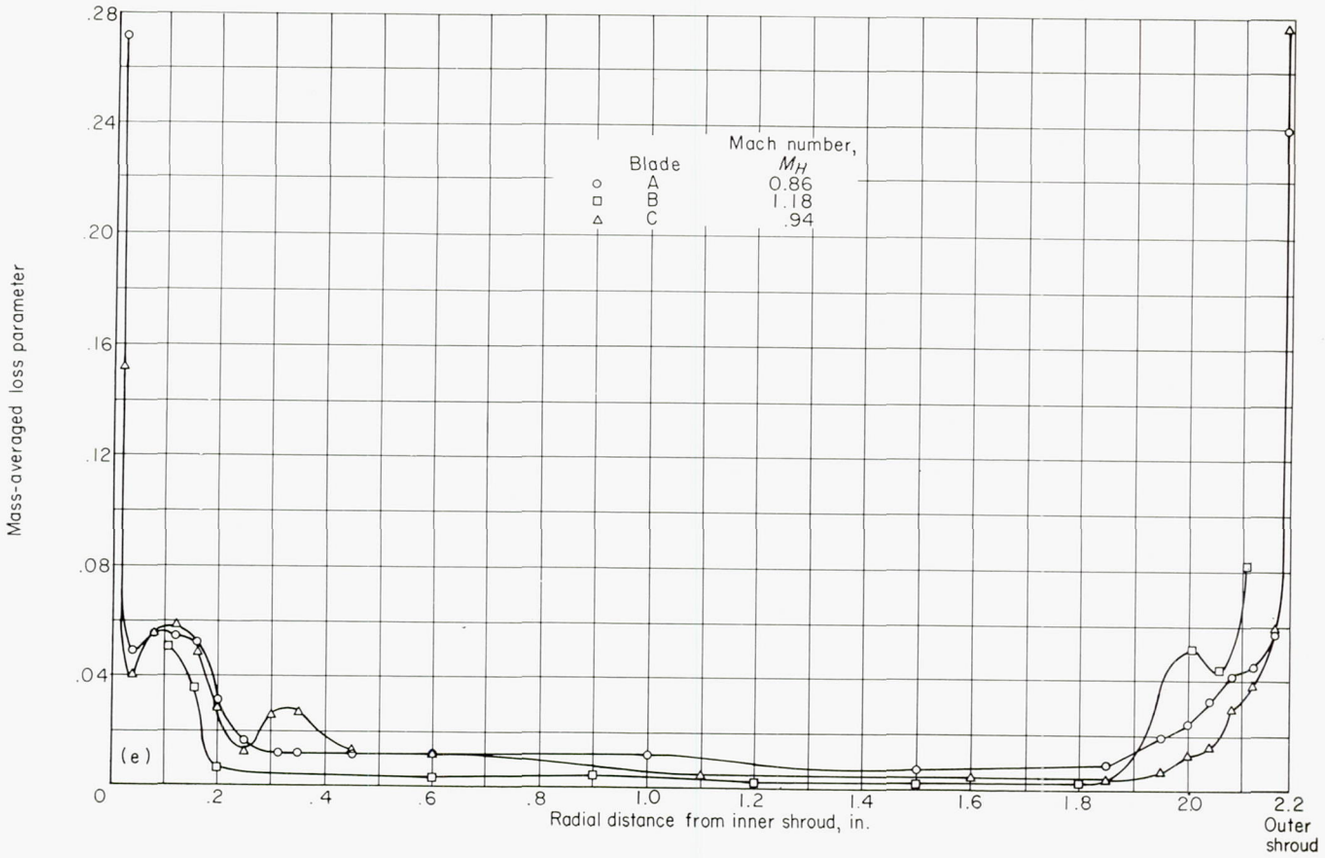

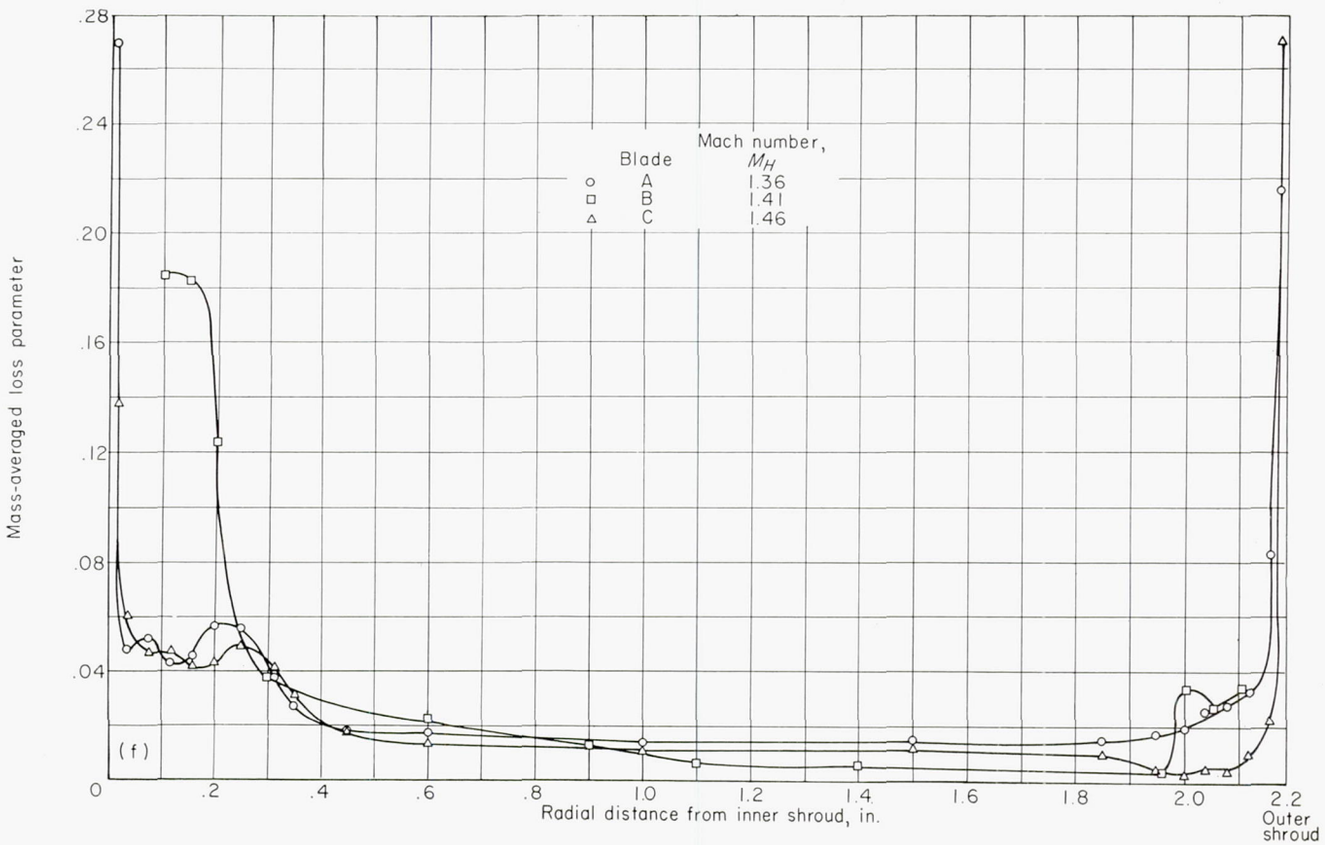

(e) Comparison of blades A, B, and C at lower Mach numbers.
(f) Comparison of blades A, B, and C at higher Mach numbers.

FIGURE 10.—Concluded. Radial distribution of loss at nozzle discharge.

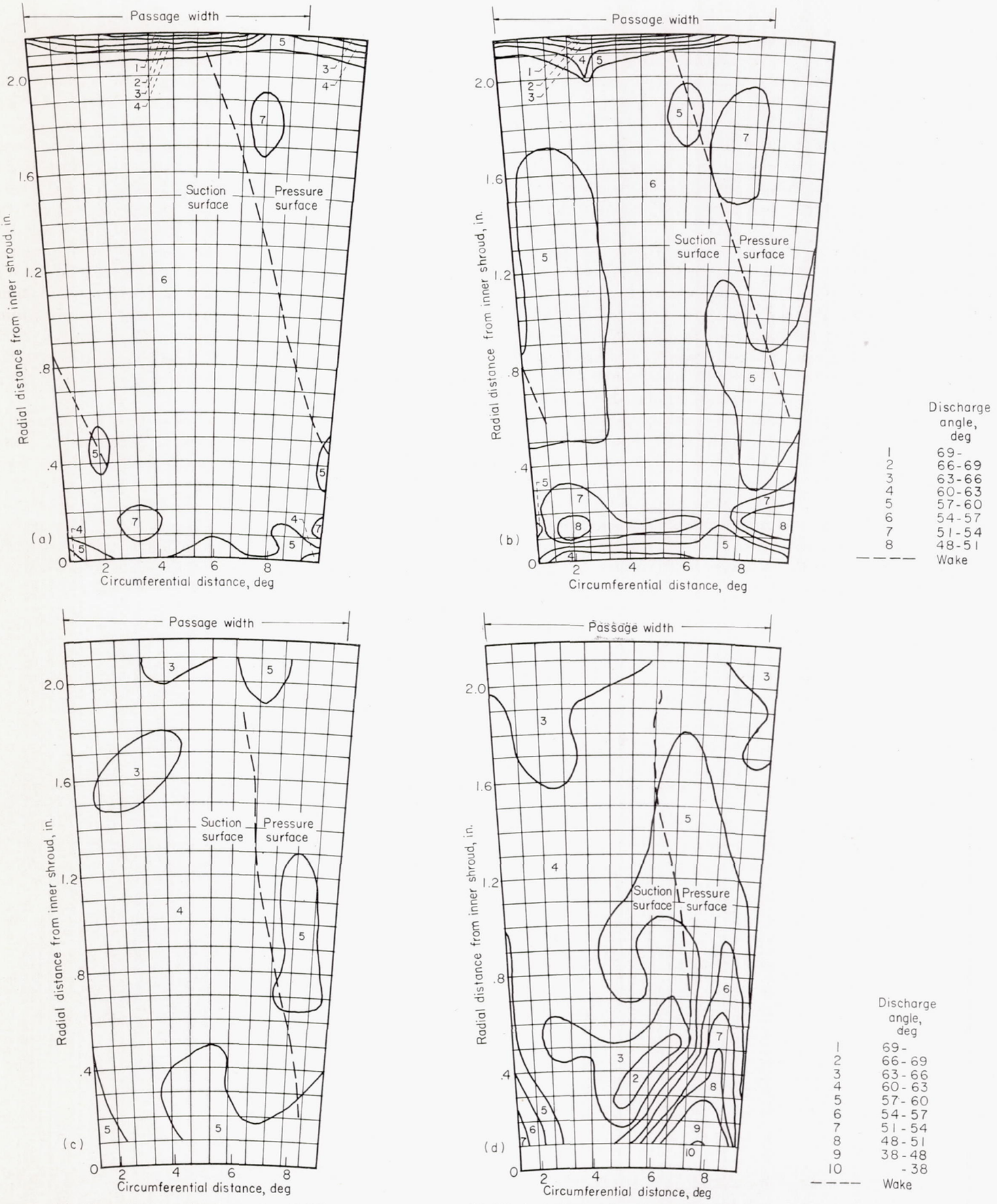

(a) Blade A; lower Mach number (0.86). Design discharge angle, 56°

(b) Blade A; higher Mach number (1.36). Design discharge angle, 56°.

(c) Blade B; lower Mach number (1.18). Design discharge angle, 59.75°.

(d) Blade B; higher Mach number (1.41). Design discharge angle, 59.75°.

Figure 11.—Contours of discharge flow angle across one blade passage.

295668—54——3

the hub this decrease was more pronounced for the higher than for the lower Mach number. The reverse was true for the decrease near the outer shroud. This difference is attributed to a combination of Prandtl-Meyer expansion and increased accumulation of low-momentum fluid near the inner shroud at the higher Mach number, which effectively blocked the flow and induced high axial velocities in the immediate vicinity. This is discussed more fully in reference 12. Also, at points nearer the walls the discharge angle increased, showing overturning in the boundary layers at the measuring station.

Discharge angles for blade A.—The results of the discharge-angle surveys for blade A are shown as contours in figures 11 (a) and (b). Angle gradients for the lower Mach number were negligible over most of the passage. However, they were greater for the higher Mach number. The variation in discharge angle across the passage at a radial distance of 0.1 inch from the inner shroud increased from 4.1° for the lower Mach number to 8.9° for the higher Mach number. In each case the greatest variation in discharge angle outside the boundary layers occurred in the large loss regions typically found near the inner shroud in all nozzle configurations.

Radial plots of the circumferentially mass-averaged discharge angles (figs. 12 (b) and (c)) for blade A show the same relations for measured discharge angle to design values as were obtained for blade C.

Comparison of discharge-angle distributions in blades A, B, and C.—Contour plots of discharge angles (fig. 11) and radial plots of mass-averaged discharge angles (figs. 12 (b) and (c)) show good agreement at the lower Mach numbers over most of the passage between design and measured angles for blades A and C and fair agreement for blade B. At these lower Mach numbers, the only severe angle gradients were in the boundary layers. At the higher Mach numbers, the contour plots show the effects of considerable disturbance in the direction of discharge flow distributed through the passage for all three blades, although blades A and C show mass-averaged values that are still near design values over most of the passage. Blade B at the higher Mach number shows severe angle gradients in the inner-shroud loss region, with underturning amounting to as much as 22° and overturning of about 8°. At a radial distance of 0.1 inch from the inner shroud, the circumferential variations in measured discharge angles were 4.1°, 2.4°, and 2.6° for blades A, B, and C, respectively, at the lower Mach numbers. At the higher Mach numbers the corresponding variations were 8.9°, 25.0°, and 9.5°, respectively.

For blades A and C, as either shroud was approached (figs. 12 (b) and (c)), there appeared decreases in mass-averaged discharge angle relative to design value. Near inner shrouds, a decrease also appeared for blade B. The decreases near the inner shroud were more pronounced at the higher Mach number, whereas near the outer shroud the decreases were smaller for the higher Mach number. Also, in the shroud boundary layers themselves, the discharge angle increased, showing overturning in the boundary layers

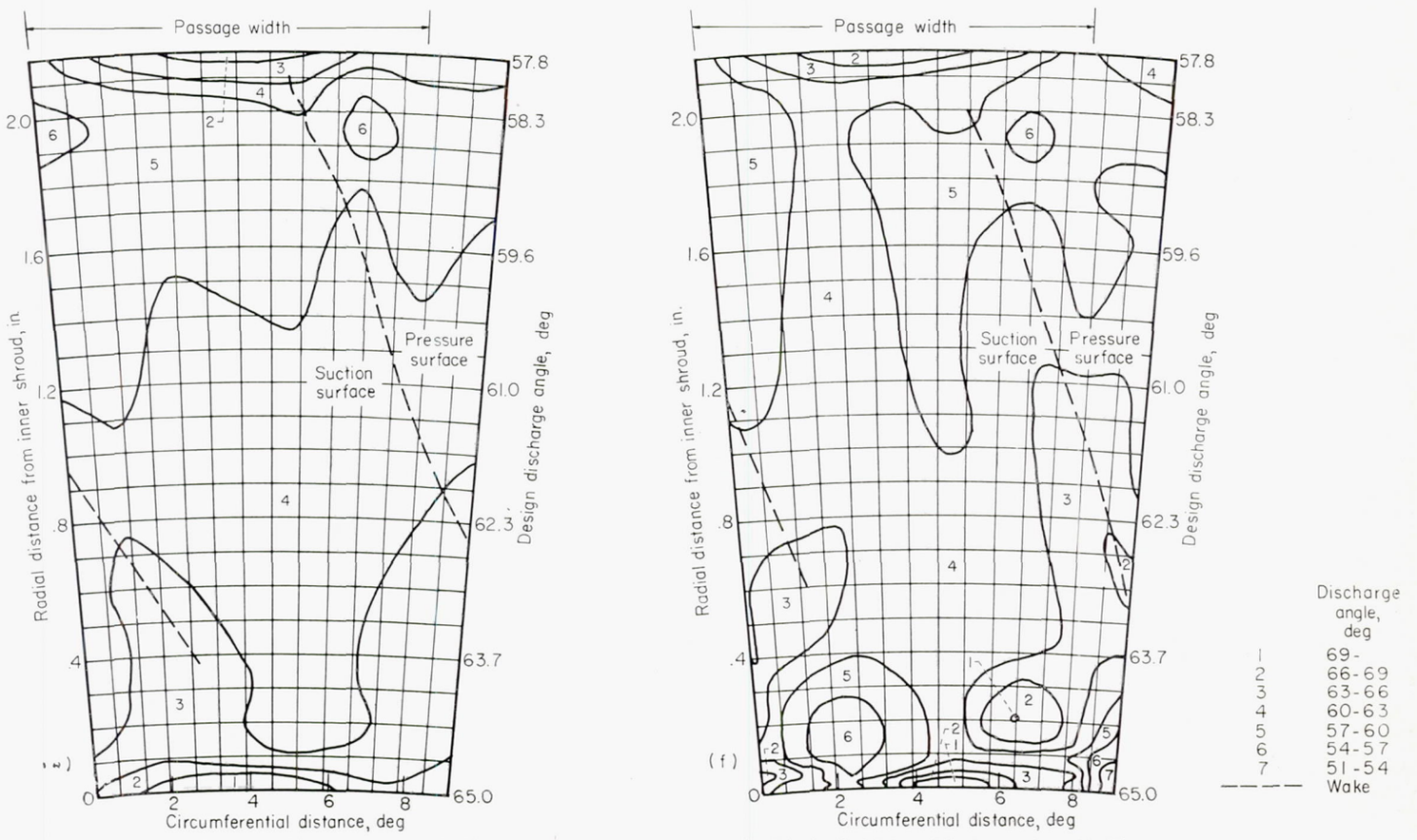

(e) Blade C; lower Mach number (0.94).

(f) Blade C; higher Mach number (1.46).

FIGURE 11.—Concluded. Contours of discharge flow angle across one blade passage.

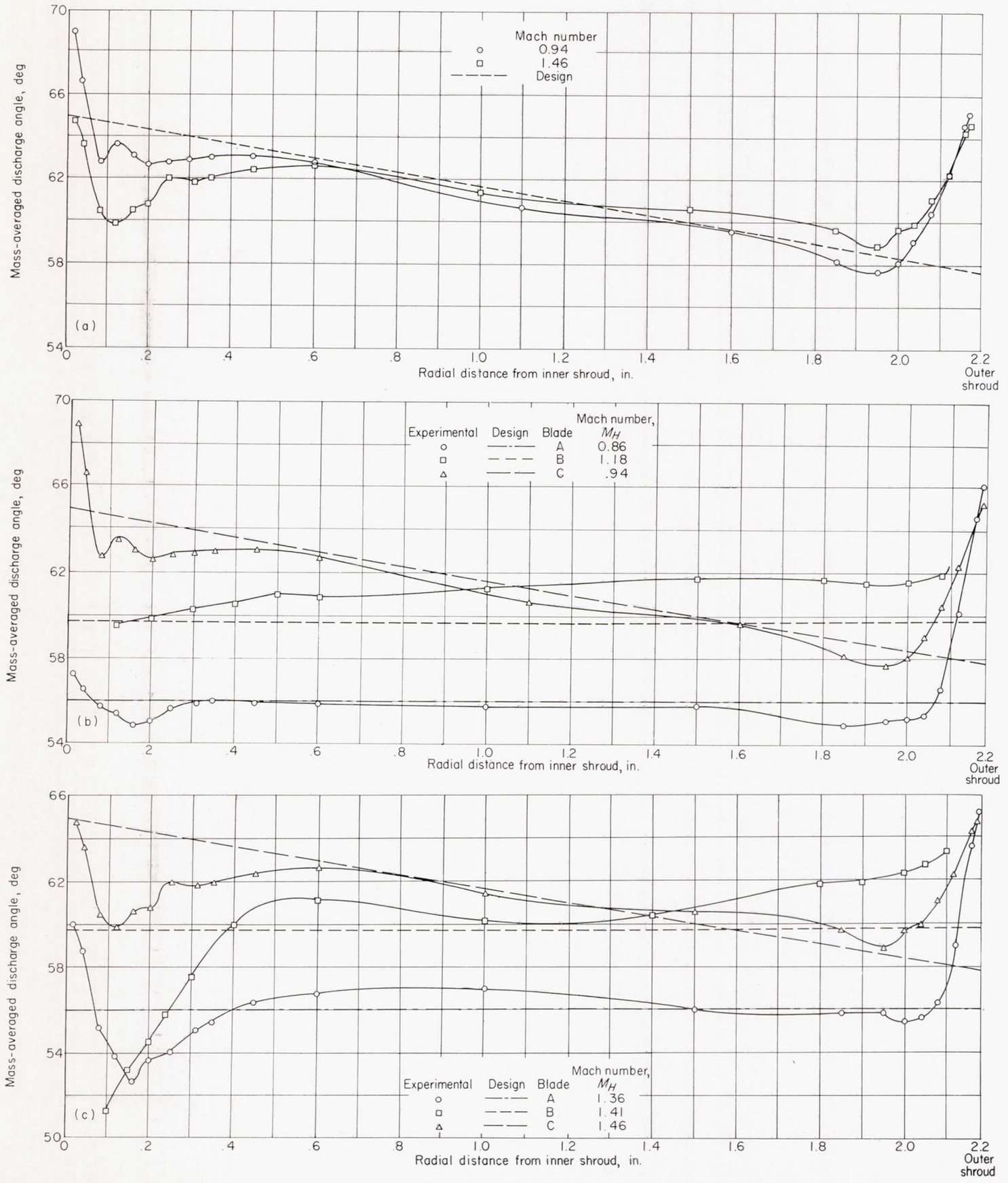

(a) Blade C.
(b) Comparison of blades A, B, and C at lower Mach numbers.
(c) Comparison of blades A, B, and C at higher Mach numbers.

FIGURE 12.—Radial distribution of mass-averaged discharge angle.

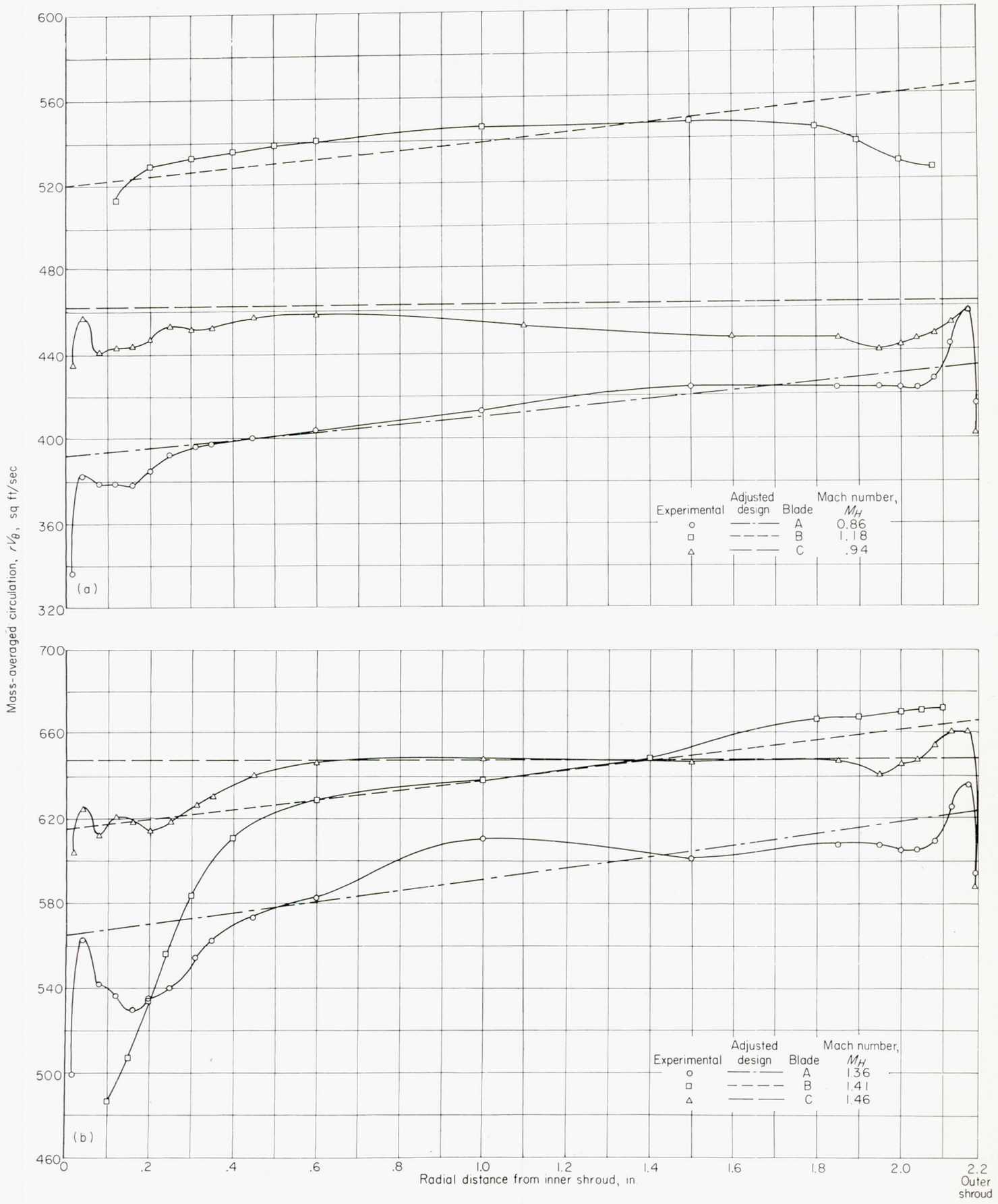

(a) Lower Mach numbers.
(b) Higher Mach numbers.

FIGURE 13.—Comparison of radial distributions of circulation.

CIRCULATION DISTRIBUTIONS

Adjusted design and measured spanwise variations in mass-averaged circulation are shown in figure 13 for the three sets of blades at the two Mach numbers. As design and measured Mach numbers are approximately the same at the lower Mach number run for blade C, design and actual spanwise circulation can be compared directly. For the other cases, design and actual Mach numbers are different, and the design circulation in each case was therefore adjusted in magnitude to provide agreement with the measured values while maintaining the correct ratio between outer-shroud and inner-shroud circulation for that design. This was done to emphasize any variations in experimentally determined spanwise circulation resulting from secondary-flow effects.

The variations of mass-averaged circulation obtained from measurements are seen to be in good agreement with the adjusted design variations through the greater part of the passage. However, in the boundary layers of blades A and C where the discharge-angle measurements are available and indicate considerable overturning, the experimental circulation increased as the shroud was approached. This continued to the point where the velocity in the boundary layer became small enough to overbalance the effect of discharge-angle increase. At this point the circulation began to decrease rapidly. In loss regions, also, experimental values of circulation were affected by the low velocities and the high discharge-angle gradients. An extreme example of this effect appears in figure 13 (b) for blade B, where the experimentally obtained mass-averaged circulation decreases approximately 20 percent from its midspan value as the inner shroud is approached.

Figure 13 also shows that the design spanwise distribution of circulation is not greatly different for the two types of blade design, vortex and constant discharge angle.

SURFACE FLOW TRACES

Blade C surface flow visualization.—Visual patterns of shroud cross-channel boundary-layer flows for blade C (ref. 5), obtained by the use of hydrogen sulfide traces on white lead paint, are presented in figure 14. A view of the cascade inner shroud at the blade-row inlet is shown in figure 14 (a). The dark hydrogen sulfide traces indicate that the gas was admitted through a wall static tap in each of two adjacent passages. At the outer shroud, the hydrogen sulfide was admitted through a single inlet static tap near the pressure surface of a blade. The downstream views (figs. 14 (b) and (c)) show that the boundary-layer flow crossed the channel completely and flowed onto the blade suction surface at both the inner and outer shrouds. The cross-channel deflection pattern was the same at both flow Mach numbers.

The results of the use of a free-flowing paint to trace the radial components of flow at the higher Mach number are shown in figures 15 and 16. Figure 15 shows how a line of flow discontinuity (or shock) along the outer shroud from the trailing edge of the pressure surface crosses the channel and continues radially inward along the suction surface of the blade. The intersection of this shock and the boundary layer on the blade suction surface results in a thickened boundary layer there and a sizable region extending from

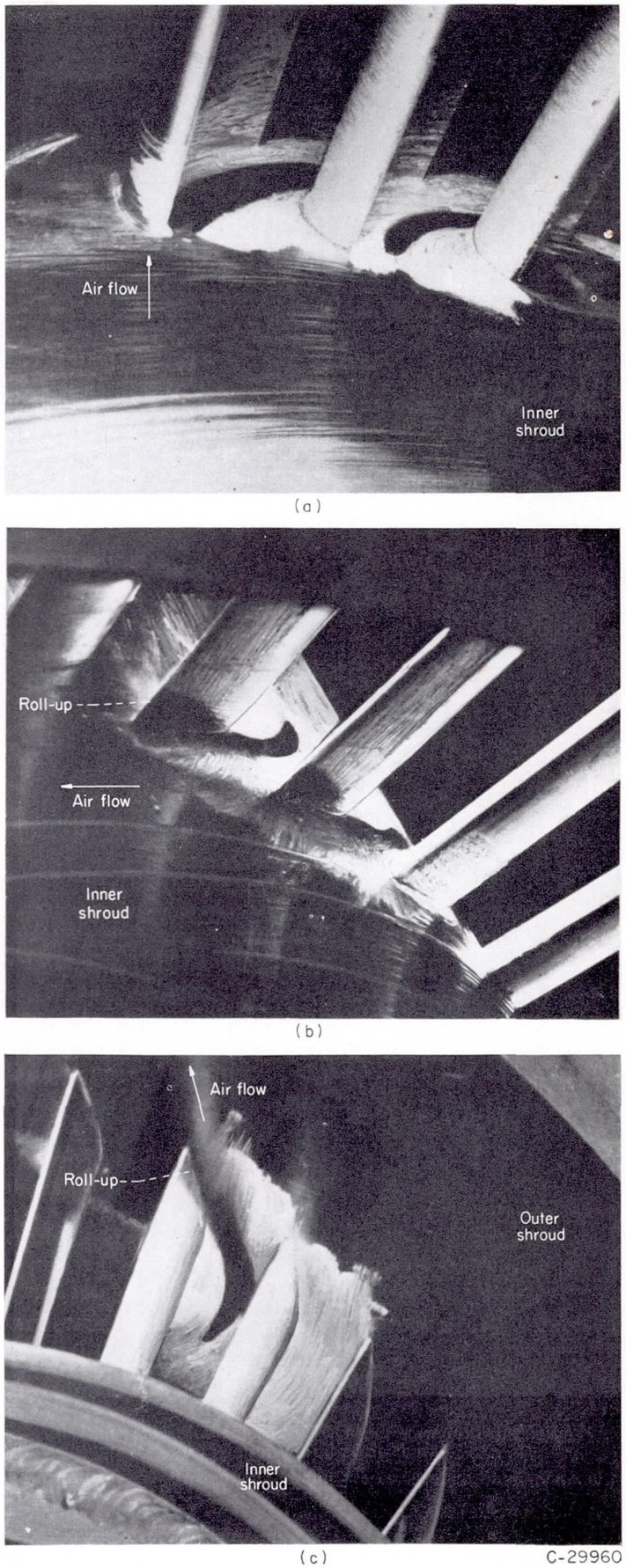

(a) Inner shroud at inlet. (b) Inner shroud at discharge.
(c) Outer shroud at discharge.

FIGURE 14.—Hydrogen sulfide flow traces through blade channel.

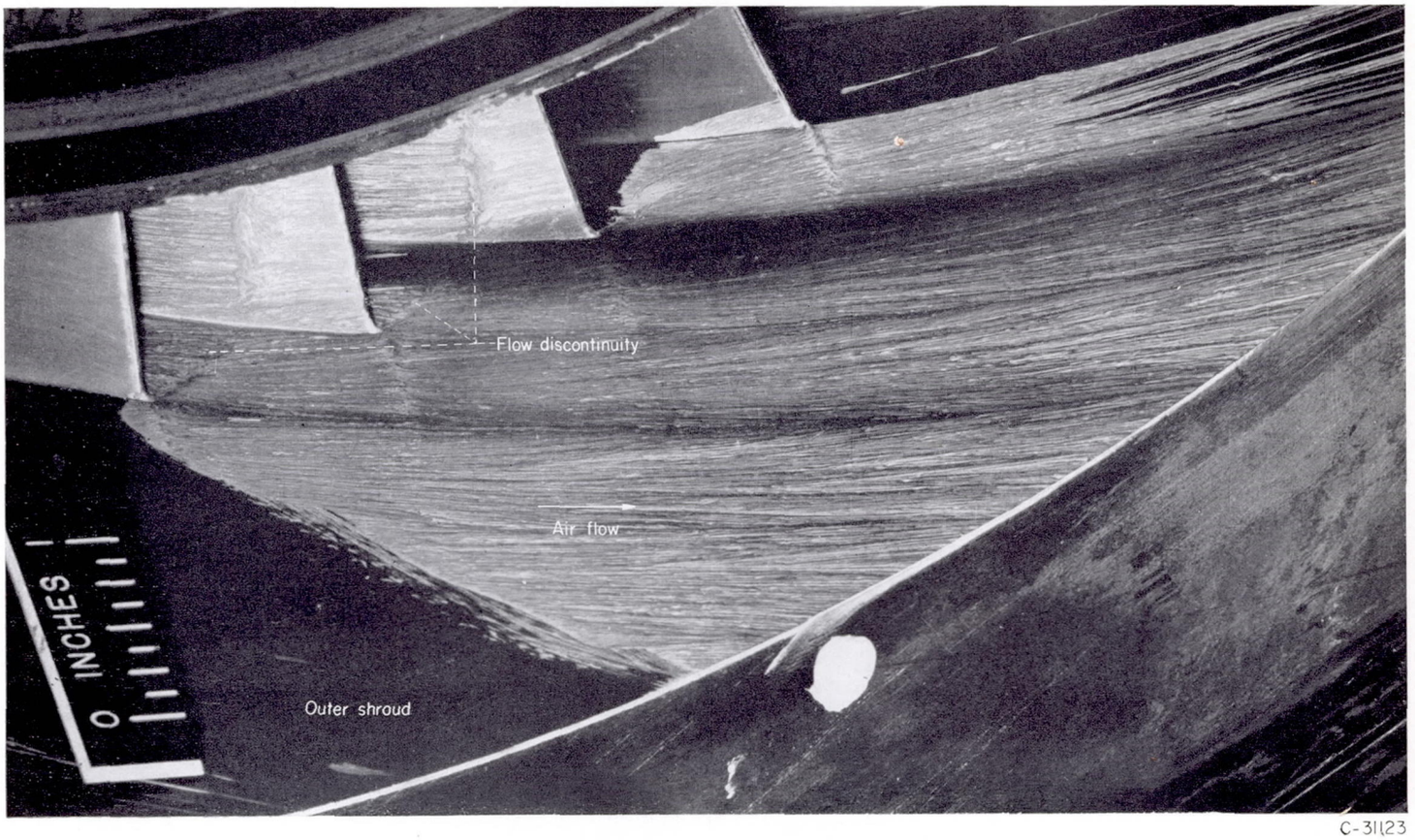

FIGURE 15.—Flow discontinuity at nozzle discharge.

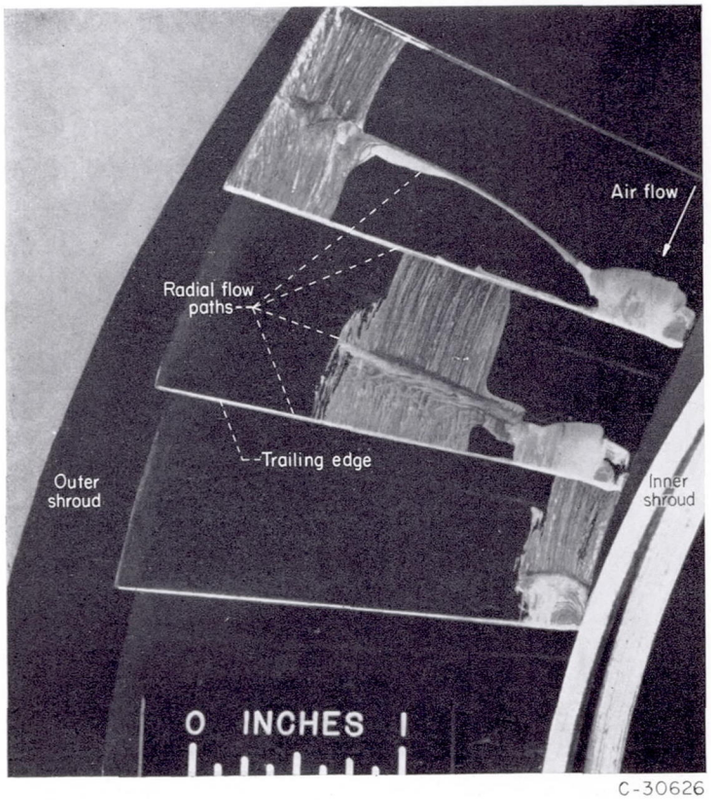

FIGURE 16.—Paint traces on suction surfaces of blades. Hub Mach number, 1.46.

tip to hub in which the through-flow velocities are small (fig. 17 (b)), similar to the situation behind the blade trailing edge. This suction-surface region of thickened boundary layer and the region behind the blade trailing edge provide flow paths through which boundary-layer material could flow radially inward because of the radial pressure gradients in an annular-nozzle cascade. Figure 16 shows paint-trace patterns made by the radial boundary-layer flow components in the suction-surface region. Narrow bands were painted on the suction surfaces of the blades at three radial locations—near the outer wall, at midspan, and near the inner wall. The radial flow of paint from the outer to the inner wall provided indications of the radial flow from the outer- to the inner-wall regions.

Blade A surface flow visualization.—Figures 18 and 19 present hydrogen sulfide and paint traces that show the same secondary-flow phenomena for blade A as reported earlier for blade C. Figure 18 (a) shows an upstream view of hydrogen sulfide traces on the inner shroud indicating the cross-channel path of the gas from its origin in static taps near the leading edges of the blades. Similar traces were formed on the outer shroud by hydrogen sulfide gas emitted from outer-shroud static taps. Figure 18 (b) shows the same traces, viewed from downstream, as the low-momentum air accumulated on the suction surfaces near the trailing edges of the blades.

Figure 18 (c) for the lower Mach number and figure 19 for the higher Mach number present results that indicate, for blade A, radial flows of the types discussed for blade C. In figure 18 (c), blade 1 is painted at the tip on the pressure surface, blades 2 and 3 at midspan on the suction and pressure surfaces, respectively, and blades 4 and 5 at the root on suction and pressure surfaces, respectively. For each blade, the paint flowed around to the trailing edge and inward along this edge to the hub, indicating the probable existence of radial flow at the trailing edge for the lower Mach number. Figure 19 shows paint traces for the higher Mach number indicating radial flow inward along the trailing edge and also along the suction surface of the blade through the boundary layer where it was thickened by encountering a shock across the passage from the trailing edge of the adjacent blade. Blades 1 and 2 in figure 19 had their entire suction surfaces painted, and these blades show not only the flow path inward along the suction surfaces but also hydrogen sulfide traces where the low-momentum air flowed out or accumulated on the suction surfaces near the trailing edges. Blades 3 and 4 were painted near the outer shroud on their suction and pressure surfaces, respectively. Blade 3 shows the suction-surface flow path, and blade 4 shows flow down the trailing edge and around to the suction surface near the root. Blades 5 and 6 were painted at midspan on their suction and pressure surfaces, respectively, and present paint traces showing probable radial flow behind the trailing edge and in the thickened portion of the suction-surface boundary layer.

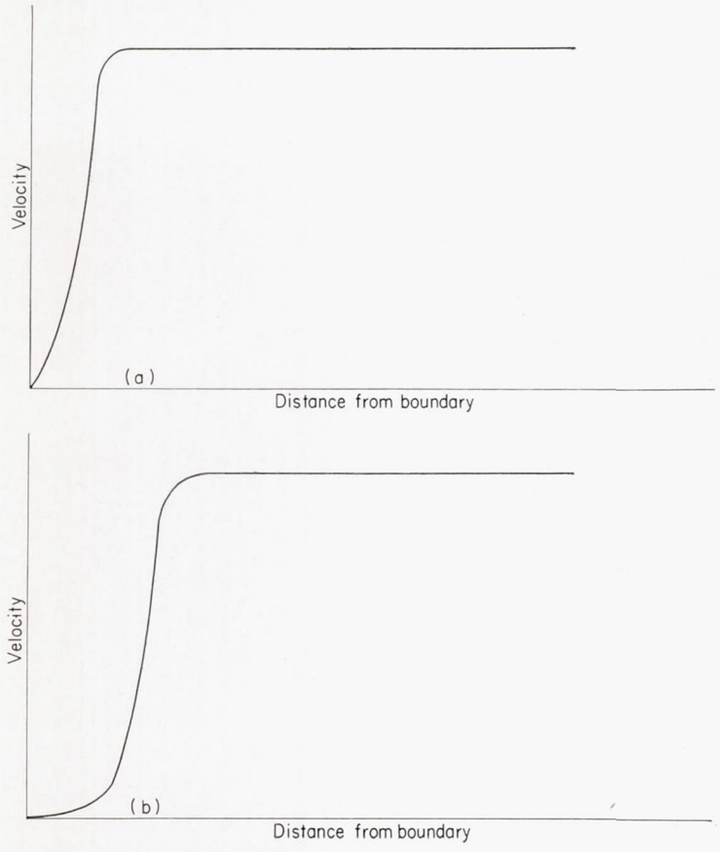

(a) Thin boundary layer.
(b) Thickened boundary layer.

FIGURE 17.—Comparison of velocity profiles for thin and thickened boundary layers.

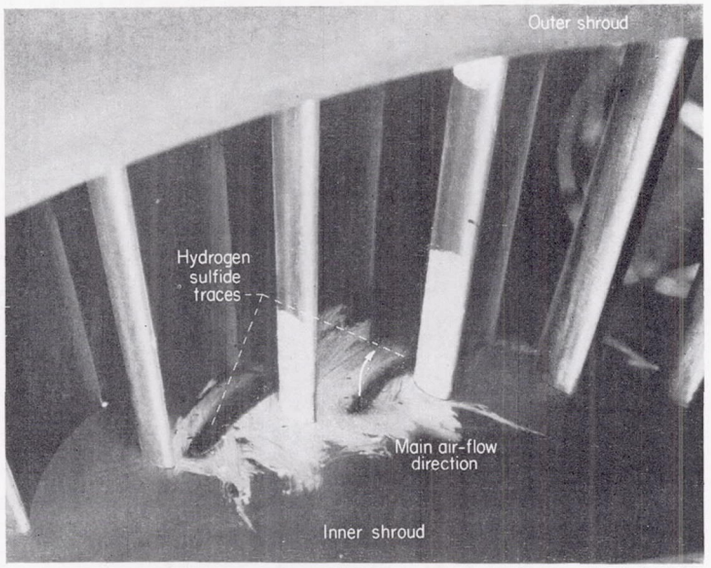

(a) C-32830

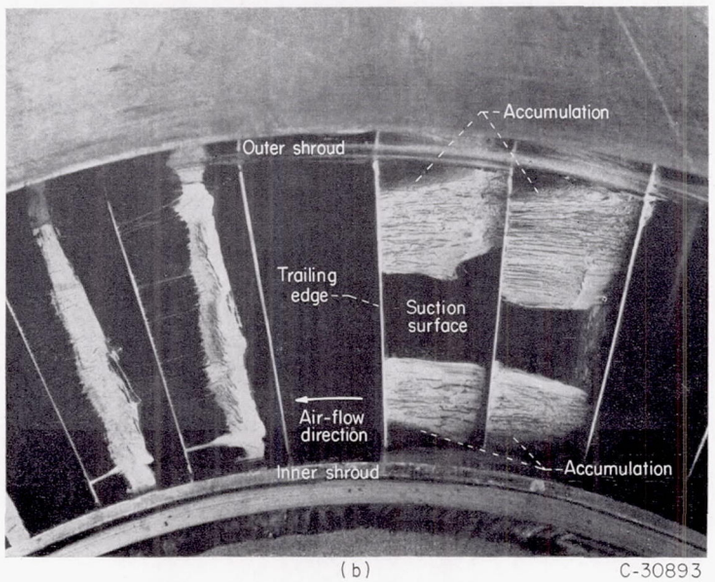

(b) C-30893

(a) Upstream view of hydrogen sulfide traces.
(b) Hydrogen sulfide and paint traces at discharge.

FIGURE 18. Hydrogen sulfide and paint traces at lower Mach number (blade A).

SMOKE FLOW-DIRECTION STUDIES

The sole purpose of the smoke flow-direction studies was to indicate any basic differences that may exist in boundary-layer and secondary-flow behavior between the two blade configurations A and B. When smoke was introduced into the flow passage in such a manner that it would enter the outer-shroud boundary layer and follow the motion of the low-momentum air through the passage, it was found that the flow paths were different for the two constant-discharge-angle blades A and B. Presumably, such differences were

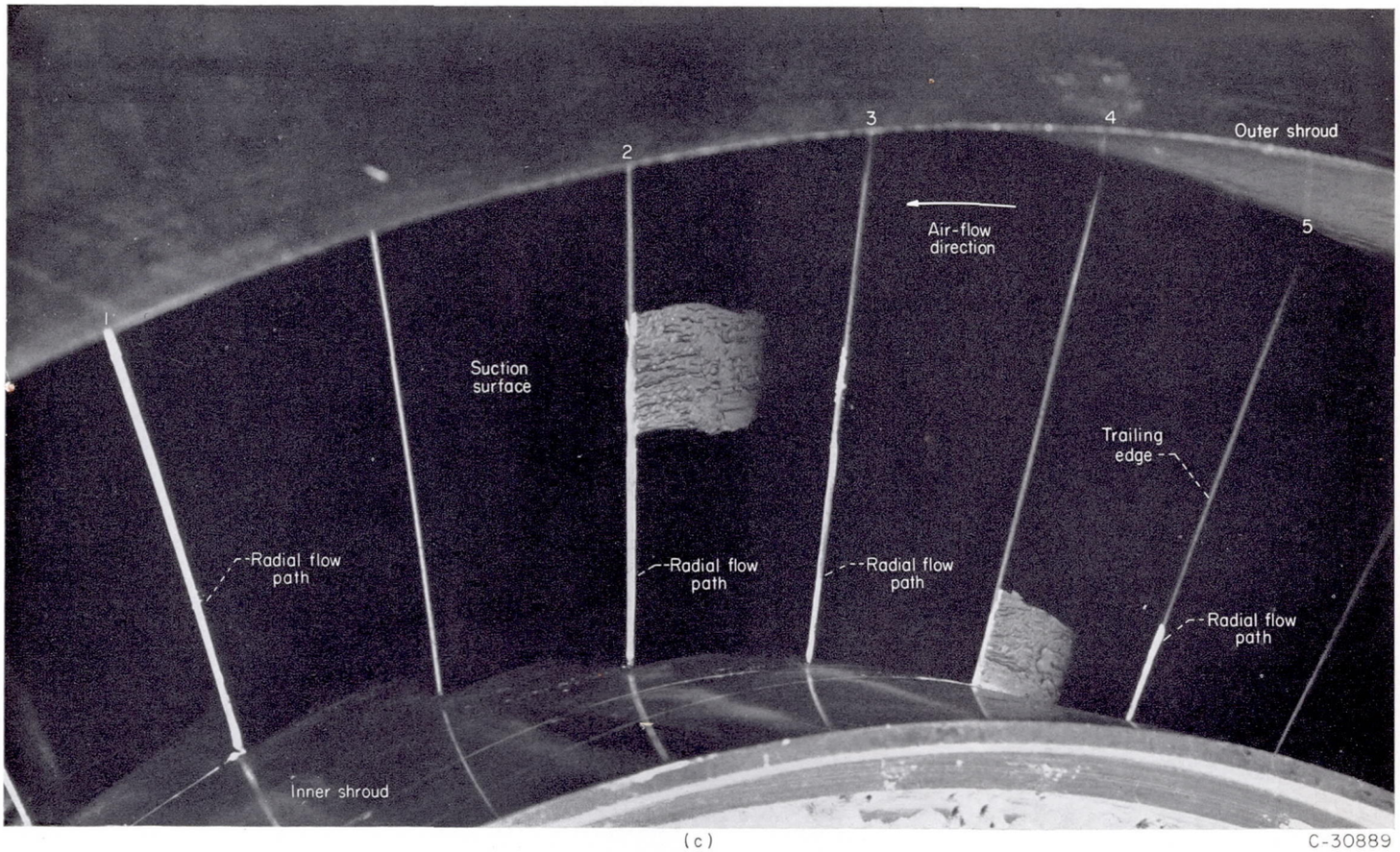

(c) Trailing-edge paint traces.

FIGURE 18.—Concluded. Hydrogen sulfide and paint traces at lower Mach number (blade A).

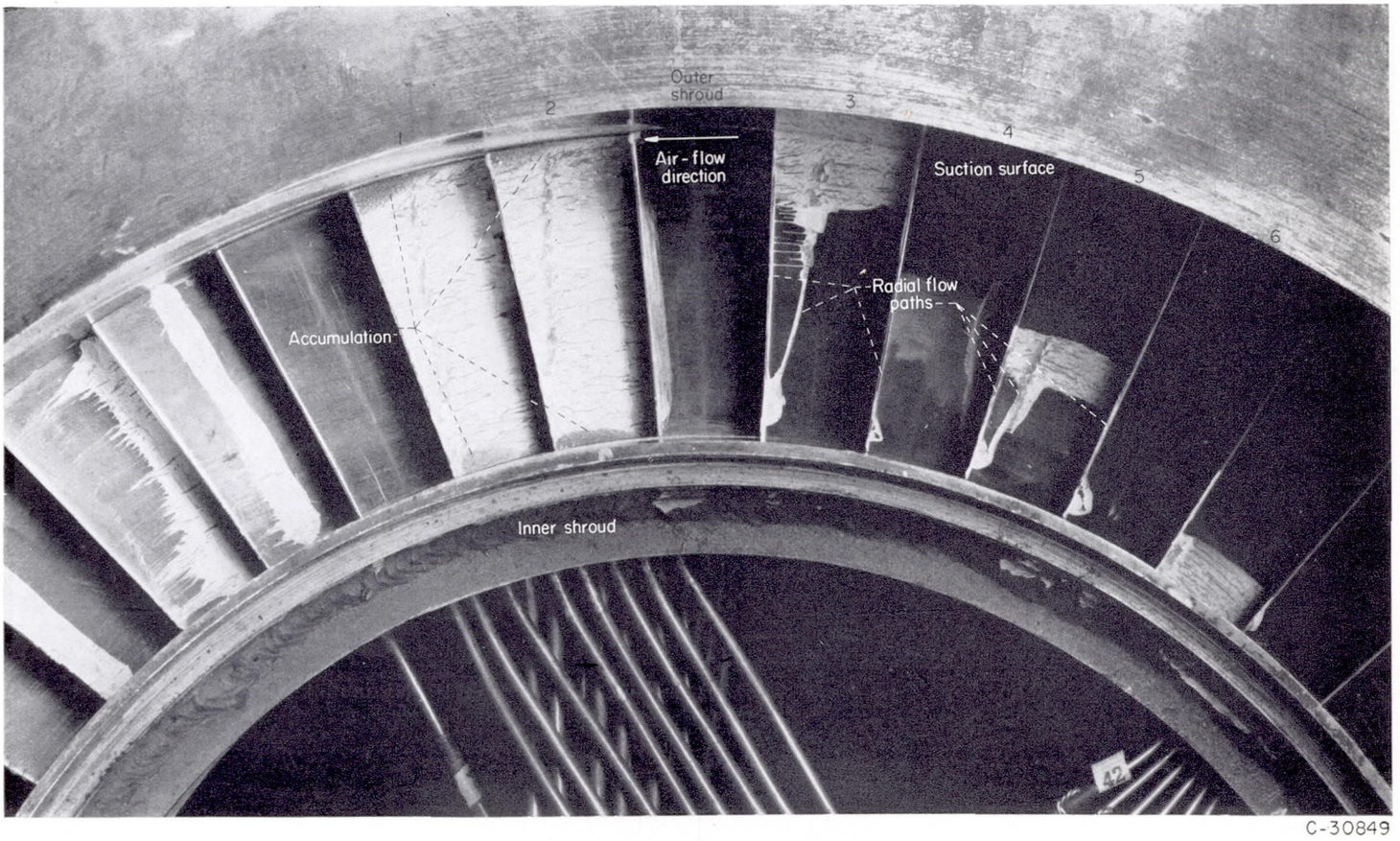

FIGURE 19.—Hydrogen sulfide and paint traces at higher Mach number (blade A).

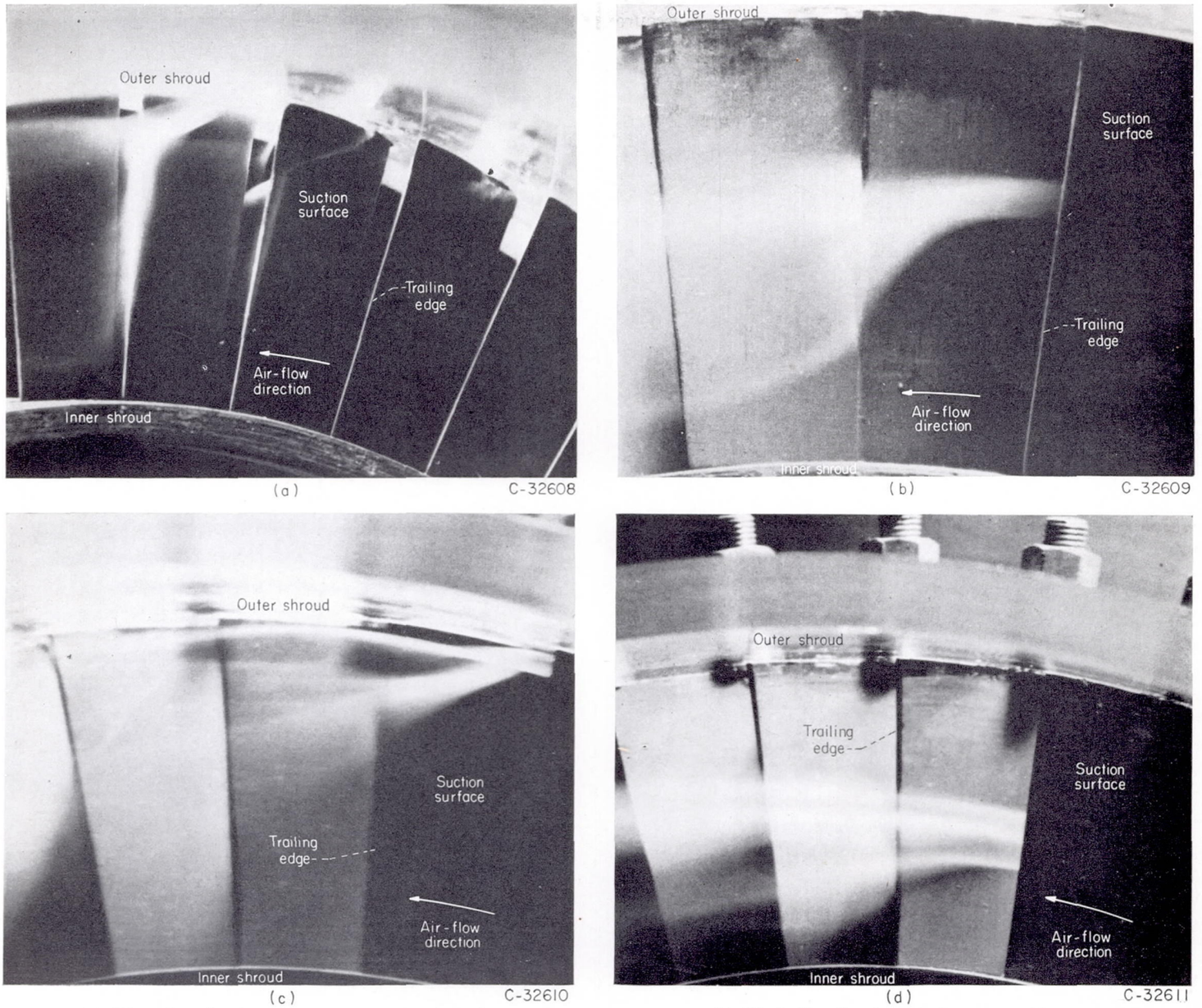

(a) Blade B. Smoke entering near outer shroud.
(b) Blade B. Smoke entering near midspan.
(c) Blade A. Smoke entering near outer shroud.
(d) Blade A. Smoke entering near midspan.

FIGURE 20.—Smoke traces.

due to the same blade characteristics that produced different surface-velocity profiles for the blades. For blade B (figs. 20 (a) and (b)), the smoke flowed against the suction surface at the outer shroud and divided as it approached the blade trailing edge, most of it rapidly sweeping on downstream near the shroud and the remainder turning sharply to follow the trailing edge. When the introduction of smoke was suddenly interrupted, that which had followed the trailing edge clung to the blade surface, eddied mildly, slowly merged with the through-flow air, and gradually disappeared. The slowness of this motion indicated that, although the picture shows a large accumulation of smoke, the fraction of outer-shroud low-momentum fluid taking this radial flow path was small.

For blade A (fig. 20 (c)), the behavior was different, in that no such eddying in a large stagnant region was found. Instead, while the smoke showed a rapid radial flow component, it also had a rapid through-flow component on the suction surface, so that it was largely swept out into the wake at points somewhat removed from the outer shroud. Likewise, the smoke showed this difference between the flow behavior of the two blades when it was introduced about midway between the shrouds (figs. 20 (b) and (d)).

DISCUSSION

Whenever turning of a fluid is accomplished, as by a cascade, a balance is established between static-pressure gradients and centrifugal forces in that fluid. In an annular cascade where three-dimensional turning is involved, there are both radial and circumferential static-pressure gradients. These pressure gradients, developed in the mainstream, are imposed upon the boundary layers of low-momentum fluid on the walls and on the blades of the cascade. One result, for example, is that turning in the shroud boundary layers (cf. ref. 5) equal to the free-stream turning is not

sufficient to maintain the balance between the pressure gradients and the centrifugal forces. Thus, more than free-stream turning of the low-momentum shroud boundary-layer fluids results. The deviations in flow direction of boundary-layer fluids from the free-stream flow directions are the so-called secondary flows. Secondary flows inevitably result from the turning of fluids having boundary layers; in annular cascades, a system of three-dimensional secondary flows must always be established.

SECONDARY-FLOW PATTERNS IN BLADE C NOZZLE CONFIGURATION

Cross-channel secondary flows.—The result of overturning and cross-channel deflection of the shroud boundary layers is a thinning of the shroud boundary layers at the pressure surface and a thickening at the suction surface, where a tendency toward the formation of regions of low-momentum fluid occurs and where the tendency for flow separation is greatest. The loss contours shown in figures 8 (e) and (f) indicate the boundary layers to be thinnest on the pressure side of the wake and thicker toward the suction surface along both shrouds. A visual picture of the cross-channel secondary flow and the accumulation of low-momentum air in the corner between shroud and suction surface is shown in figure 14. The dark hydrogen sulfide trace appearing between the blades in the view from the inlet side (fig. 14 (a)) indicates the source of the gas to be a static tap near the pressure surface at the leading edge. This view is at the inner shroud; a source at the outer shroud was in a similar position. Figure 14 (b) shows the hydrogen sulfide trace from downstream as it rolls up with the low-momentum air on the suction surface of the blade at the inner shroud, having traversed the passage in the boundary layer from its source near the pressure surface of the adjacent blade. Similar results were found at the outer shroud, as shown by figure 14 (c) in a downstream view of the trailing edge of the blades at the intersection of their tips with the shroud.

The mechanism of the cross-channel secondary flow in nozzle-shroud boundary layers and the significant flow parameters involved are discussed in reference 5. It must be noted carefully that these surface flow-trace tests cannot by themselves prove whether "passage vortex" formation—the roll-up of the shroud boundary layer into a discrete flow vortex at the suction side of the passage—has taken place or not.

Radial flows at lower Mach number.—Just as the cross-channel pressure difference induces a deflection of the flow toward the low-pressure side of the passage, so the pressure difference existing between outer and inner shrouds can be expected to induce radial flow through blade boundary layers and wakes. An examination of the loss cores in the measuring plane at both flow conditions (figs. 8 (e) and (f)) discloses that the loss region measured at the outer wall is smaller than that at the inner wall. Because the "wetted area" of the outer wall is the larger, the relative magnitudes of the inner and outer loss regions indicate the presence of radial flows in the blade boundary layers and wake regions.

In general, the boundary layers in the turbine nozzle cascade are thin; a typical velocity profile is shown in figure 17 (a). The high through-flow velocities existing in all but very small regions in such thin boundary layers tend to prevent any sizable transport of material from the tip to the hub. In order for quantities of low-momentum fluid to flow the entire distance from the outer wall to the inner wall, there must exist some sizable regions, extending from tip to hub in a passage, in which the through-flow velocities are small (fig. 17 (b)). This situation occurs in the wake of the blade.

During the tests to trace the cross-channel secondary flow on the outer wall, faint traces of hydrogen sulfide flowing radially down the trailing edges were noted. These traces, coupled with the observation that there seems to be no a priori reason for the loss core at the inner wall to be so much larger than at the outer wall for these blades (figs. 8 (e) and (f)), were considered to indicate radial transport of fluid at the lower Mach number. One possibility was that radial flow in sufficient quantities to cause part of this difference in inner- and outer-wall loss cores might occur along the blade suction surface where the paint traces showed some indication of flow separation.

It was noted in reference 5 that, once the so-called passage vortex is formed as a result of cross-channel deflection, it tends to resist turning as it proceeds downstream. Therefore, the absence of a sizable loss core near the outer shroud at this flow condition (lower Mach number) not only indicates the presence of radially inward flows of boundary-layer fluids, but also possibly indicates that the accumulation of boundary-layer fluid at the suction surface does not, in this case, roll up into such a well-defined vortex. It is conjectured that the radial pressure gradient serves to prevent vortex roll-up by draining the boundary-layer fluid radially toward the inner shroud almost as rapidly as it reaches the suction surface.

Radial flows at higher Mach number.—An examination of the loss cores in the measuring plane at both conditions (figs. 8 (e) and (f)) discloses that the loss region measured at the outer wall at the higher Mach number was actually smaller than that at the lower Mach number. This result was considered evidence that more of the low-momentum fluid must flow radially toward the inner wall on the blade or in the blade wake at the higher Mach number. Flow visualization by means of paint traces strongly suggests that at least part of the increased radial flow results from the availability of new or larger hub-to-tip radial flow paths at the higher Mach number.

Figure 15 shows for the higher Mach number a line of flow discontinuity (or shock) along the outer shroud from the trailing edge of the pressure surface across the channel, which continues inward along the suction surface of the adjacent blade. The intersection of the flow discontinuity and the boundary layer on the suction surface of the blade results in a thickened boundary layer. The low viscous shear forces in the thickened boundary layer and the presence of a radial pressure gradient provide a region and inducement for the inward radial flow of low-momentum fluid from the outer to the inner shroud.

Free-flowing-paint tests on vortex blade C were conducted with results so nearly identical to those obtained for blade A (figs 18 (b) and (c), and (19)) that the discussion of

these results as presented for blade C is considered equally valid for blade A.

An enlarged view of the inward radial movement of the low-momentum fluid at the higher Mach number is given in figure 16. Suction surfaces and trailing edges are shown. In the tests made for this photograph, three blades were involved. Strips of paint were applied to the suction surfaces of the blades near the inner shroud, at the midsection, and near the outer shroud. The paint traces represent the flow of low-momentum fluid in the thickened boundary layer resulting from the intersection of blade surface and flow discontinuity, as well as the flow along the trailing edge of the blade in the wake. The pattern also shows evidence of backflow in part of this region.

The shift of the major loss region from the outer part of the passage to the inner with increasing Mach number and the paint traces of flow at the higher Mach number give good indications that low-momentum fluid originating on the outer shroud and on the blade surfaces flows radially inward along the line of flow discontinuity as well as along the trailing edge in the blade wake. The radially inward motion of the low-momentum fluid is accomplished through boundary-layer regions of reduced viscous shear forces in the presence of the radial pressure gradient.

Over-all sketch of secondary-flow paths.—Figure 21 is a sketch showing the secondary-flow paths in the annular cascade, as indicated by the flow measurements and visual traces. According to this sketch, much of the low-energy material in a loss core near the blade inner shroud originates elsewhere in the passage. Some of it originates on an adjacent blade and, along with the inner-shroud boundary layer, becomes part of this loss core by cross-channel deflection. Another portion originates on the adjacent blade near the outer shroud. This blade boundary-layer material, together with some of the outer-shroud boundary layer, deflects across the channel along the outer shroud and then flows radially along the indicated paths on the blade to become part of the loss core near the inner shroud.

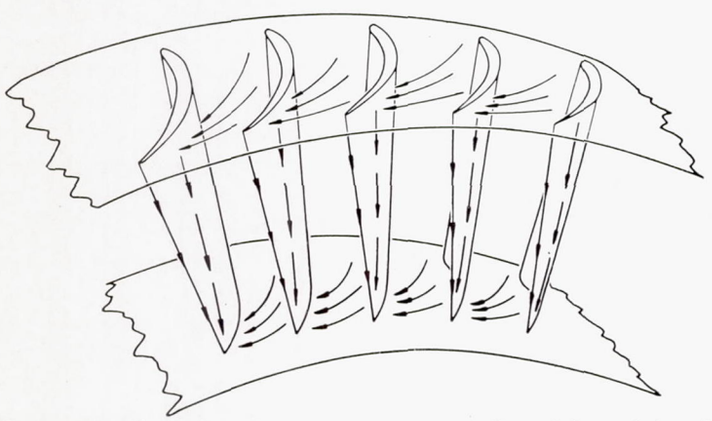

FIGURE 21.—Secondary-flow components as indicated by paint and hydrogen sulfide traces. Hub Mach number, 1.46.

EVALUATION OF RADIAL SECONDARY-FLOW COMPONENTS IN BLADE C NOZZLE CONFIGURATION

The investigation described in this section was undertaken in an effort to learn more about the origin and the disposition of secondary flows and, in particular, to verify the preceding indications that flow losses originating at the outer wall comprise a portion of the losses measured at the inner wall. The blades were modified in an effort to interrupt the secondary flows in such a manner as to enable evaluation of their components. The investigation was principally concerned with the effects of various modifications on the radial transport of low-momentum fluid to the inner-wall region. Consequent changes in the size of the loss core at the inner wall were used to evaluate the results.

Preliminary considerations.—The reasons for using the changes in size of the inner-wall loss cores as criteria for evaluating the effectiveness of the modifications are as follows. In general, it was observed that the sheet-metal fences on the blades were effective in blocking the radial flows. (The criterion applied was the effectiveness in reducing the accumulation of low-momentum fluid at the inner wall.) Because the fences increased the wetted surface area in the flow passage, the modifications themselves introduced some viscous losses. Separation of these modification-induced losses from the low-momentum fluid interrupted by the modifications is not readily feasible. Accordingly, the changes in size of the inner-wall loss core are used as criteria for evaluating the effectiveness of the modifications and as a basis for interpretation of the results. As expected, none of the modifications used affected the losses near the outer wall under any condition, being "downstream" of the outer wall with respect to the radial flows.

Full-flow-fence modification at hub Mach number 0.94.—Only the full-flow-fence modification was used for flows with a hub Mach number of 0.94. Comparison of figures 9 (a) and 8 (e) shows that the flow fences apparently had a negligible effect on the inner-wall loss core. Examination of figure 10 (b) also shows this factor in terms of the circumferentially averaged loss from the inner wall to the fence. As noted earlier, the discrepancy in the relative sizes of the inner- and outer-shroud loss cores indicates that radial transport of boundary-layer material probably does occur; but there was no evidence from these tests at the lower Mach number flow to show the location or quantity of this transport. However, if it does take place, there are indications that it occurs chiefly along the suction surface upstream of the flow fence. The losses that appear at the flow-fence position, approximately 1.1 inches from the inner wall, evidently are generated by the fences themselves.

Full-flow-fence modification at hub Mach number 1.46.—The existence of radial flows that would enable transport of low-momentum fluids from the outer to the inner wall was investigated, and measurements were made of the quantities involved at a hub Mach number of 1.46.

The effectiveness of the full flow fence at the higher Mach number is demonstrated by a comparison of figures 9 (b) and 8 (f). The sharp reduction in size of the inner-wall loss core as a result of the flow fences constitutes proof of radial flow and transport of low-momentum fluids from the outer to the inner wall. By integration, it was determined that approximately 65 percent of the losses that appear in the inner-wall loss-core region (0.040 to 0.500 in. from the inner wall) come from the neighborhood of the outer wall, by means of radial flows in the blade wakes and on that part of the blade surface intercepted by the fence. These estimates are

only qualitative because of the probe errors discussed in the section on **PROCEDURES**, but the over-all picture is unmistakable. The circumferentially averaged loss, plotted radially over one-half the blade height in figure 10 (c), shows the change in loss distribution effected at various radial positions by the flow fences.

The circumferential location at various radial positions of the wake in figure 8 (f) indicates underturning in the region near the hub. Comparison of figure 8 (f) with figures 9 (b) and (c) shows that the blade fences effected a reduction in the underturning in this region as well as a reduction in the size of the loss core. This reduction is evidenced by the shift in circumferential position of the loss region near the inner wall. Evidently, a large part of the underturning in that region of the unmodified cascade is caused by flow blockage due to the accumulation of low-momentum fluid.

Reduced-flow-fence modification at hub Mach number 1.46.—A further refinement of the pattern of distribution of the low-momentum fluid is provided by the reduced flow fence (fig. 9 (c)), which, by acting upon the flow in the blade wakes only, enables an evaluation of the uninterrupted flow through the thickened boundary-layer region where the shock wave abuts the blade suction surface. Thus, of the low-momentum fluid that accumulates in the loss core at the inner wall, about 30 percent is derived from radial flow through the strip of thickened blade boundary layer and about 35 percent from flow through the blade wake.

It is further shown that, in this particular cascade of nozzle blades, the thickened boundary-layer region is comparable in size to the blade wake. This fact is evident from considerations of the static-pressure gradients and the fluid densities involved, which are not greatly different in the two regions. Therefore, the quantities of flow through these regions are established as measures of the comparative sizes of thickened boundary layers and blade wakes.

3/16-Inch-notch modification at hub Mach number 1.46.—A 3/16-inch notch cut into the trailing edge of the blade (fig. 9 (d)) was not deep enough to intersect the thickened boundary-layer strip on the blade (fig. 16). The notch was intended to accomplish the same reduction of the inner-wall loss core as the flow fence by providing a discontinuity in the flow path of low-momentum fluid on the blade trailing edge. It appeared likely, because of the rapid dissipation of the wake downstream of the trailing edge below the notch, that low-momentum fluid flowing from the outer wall would be swept downstream at the blade notch. This modification failed notably to disrupt the blade-wake radial flow. Instead, the blade wake and the attendant radial flows remained attached to the trailing edge. The shift in position of the loss core in figure 9 (d) (cf. fig. 8 (f)), without appreciable change in size, supports this contention.

Furthermore, it can be seen from figure 9 (d) that a few new losses were generated at the trailing-edge discontinuity, 1.1 inches from the hub. It might well have been anticipated that there would be a large flow from the pressure surface to the suction surface along the top edge of the notch in the manner of the tip-clearance losses described in figures 35 and 36 of reference 5. In these vortex blades, however, the turning is accomplished early, and the 3/16-inch notch is in the region where the blades provide mainly guidance and where little further turning of the main flow is involved. The over-all average loss for the 3/16-inch-notch modification is thus increased but slightly over that of the unmodified blades.

3/8-Inch-notch modification at hub Mach number 1.46.—A 3/8-inch notch in the blade trailing edge, which was deep enough to penetrate the region of the blade where turning is involved, intersected the thickened boundary layer caused by the shock wave in the passage. From the position and size of the losses at 1.1 inches from the inner wall (fig. 9 (e)), it is evident that the notch caused underturning. From the large increase in losses at the inner wall (cf. fig. 9 (d)), it must be concluded that large losses are generated by flow from the blade pressure surface to the suction surface at the top of the notch and that these then flow radially to the inner wall.

Remarks on secondary flows in blade C nozzle configuration.—The following results were obtained at hub Mach numbers of 0.94 and 1.46 in an investigation of an annular cascade of turbine-nozzle blades designed for a free-vortex distribution of velocity with a discharge angle of approximately 65°:

(1) High loss regions were found at the junction of the blade wakes and shroud boundary layers for the two Mach numbers. The inner-shroud loss region was much larger than the outer-shroud loss region.

(2) The over-all integrated blade efficiencies were 0.99 and 0.98 in order of increasing Mach number. Although these efficiencies are high, they are not a good index of blade performance, as the high loss regions and angle gradients occurring along the suction side of the blade and inner shroud where diffusion is the greatest could result in flow instability and induce additional viscous losses and angle gradients.

(3) Angle gradients were small for the lower Mach number run; however, they increased with increasing Mach number. Circumferential angle gradients of 13.6°, 5.4°, and 4.0° at radial distances of 0.2, 1.0, and 2.0 inches from the inner shroud, respectively, led to local variations in rotor blade angle of attack of 16.9°, 6.6°, and 11.3° for the higher Mach number run.

(4) In the region of high velocity gradients (particularly in the loss region near the inner shroud and for the higher Mach number) the accuracy of measurements of pressure and flow angle may be limited, and the interpretation of these measurements should be made with care.

(5) Secondary flows are largely responsible for the distribution of losses noted downstream of the blade row. The major result of the secondary-flow mechanism in this investigation was the formation of an inner-wall loss core.

(6) Secondary flows can be intercepted by simple barriers in the flow paths of the low-momentum fluid. Thus, the degree of underturning at the inner wall caused by blockage, which is a result of the loss accumulation by the secondary flow, can be reduced.

(7) The inner-wall loss core is an accumulation of losses which for the most part originate elsewhere in the passage. On paths leading to the loss region in the corner bounded by the blade suction surface and the hub at the blade trailing edge, low-momentum fluid is transported across channels to the suction surfaces in the wall boundary layers and radially inward in the blade boundary layers and in the blade wakes. At a hub Mach number of 1.46, the radial flows in the blade wake and the thickened boundary layer on the suction surface accounted for approximately 65 percent of the loss core, about 35 percent resulting from flow in the blade wake, and about 30 percent from flow in the thickened boundary layer. At a hub Mach number of 0.94, no information concerning radial flow in the wakes was obtained directly.

SECONDARY FLOWS IN BLADE A NOZZLE CONFIGURATION

Loss distribution.—The loss contours for blade A are similar to those for blade C to a noteworthy degree. Accordingly, the discussion of the loss contours obtained with blade C can be considered equally applicable to blade A.

Loss contours (fig. 8 (a)) at the lower Mach number for blade A indicate an outer-shroud loss region distributed over a portion of the wake in such a way as to suggest that, at the measuring plane, radial pressure gradients had forced its movement toward the inner shroud, but that its through-flow component of velocity was such as to prevent a large part from actually reaching the inner shroud. Indications of the same kind of boundary-layer flow behavior at low flow Mach numbers are seen in the photographs in figures 20 (c) and (d).

The inner-shroud loss region under these conditions is composed of inner-shroud boundary-layer air with the addition of some low-momentum air reaching it by radial flow from the blade-surface boundary layer, and the measured wake is a combination of profile loss with some low-momentum air reaching it by radial flow from points nearer the outer shroud.

At the higher Mach number, the flow is different, mainly because of the additional path for radial flow provided by shock-boundary-layer thickening on the blade suction surface (fig. 19). This seems to allow the greater part of the outer-shroud loss region to reach the inner shroud and combine with inner-shroud losses to form the large region of low-momentum fluid that appears in figure 8 (b).

The mass-averaged loss curves (fig. 10 (d)) indicate a greater loss throughout the mainstream for the higher than for the lower Mach number, even though the contour plots show that the wake is smaller. Reference to the original data gives the reason for this difference. At the higher Mach number, the loss distributed through the passage outside the wake is appreciable (about 1 percent), whereas it is negligible at the lower Mach number. This implies that at the higher Mach number a mild general flow disturbance exists in the exit air from the passage.

Secondary-flow patterns.—As a result of secondary flow for blade A, the low-momentum air in the shroud boundary layers tends to move across the passage from the pressure surface toward the suction surface and to accumulate in the corners between shroud and suction surface. This movement is indicated by the hydrogen sulfide traces of figures 18 and 19 and the loss-contour plots of figures 8 (a) and (b).

Radial pressure gradients also exist in an annular cascade of nozzle blades and will drive low-momentum fluid radially to the inner shroud wherever a region of low through-flow velocity provides a complete path. The paint traces of figures 18 (c) and 19, for example, show indications of such paths. At the lower Mach number in figure 18 (c), the paint has been swept in along the trailing edge of the blade. At the higher Mach number in figure 19, an additional path is indicated on the suction surface of the blade near the trailing edge. This pattern of secondary flow in blade A is thus quite similar to that obtained for blade C. Because a comparison of blades A and C indicates that secondary-flow differences are small, it appears that the choice of blading (vortex or constant discharge angle), based solely on secondary flows, is of negligible concern.

SECONDARY FLOWS IN BLADE B NOZZLE CONFIGURATION

Loss distribution.—As noted in the **RESULTS** section, the loss contours for blade B (figs. 8 (c) and (d)) are considerably different from those for blades A and C (figs. 8 (a), (b), (e), and (f)). Not only the large size but also the regular shape of the loss region near the outer shroud downstream of nozzle blade B at the lower Mach number is noteworthy (fig. 8 (c)). The symmetric high loss region closely surrounded by regions of considerably lower loss indicates qualitatively the existence of a core of low-momentum fluid, possibly a flow vortex.

The combination of large outer-shroud loss core, comparatively small wake, and comparatively small inner-shroud loss core at the lower Mach number indicates relatively little radial flow for blade B at these conditions. However, at the higher Mach number for blade B, the existence of considerable radial flow is indicated by the large inner-shroud loss region and the reduction of the outer-shroud loss core (fig. 8 (d)).

Secondary-flow patterns.—The hydrogen sulfide and paint-trace flow-visualization techniques were not yet employed at the time the data for blade B were obtained. Nevertheless, it can be stated that the familiar pattern of cross-channel boundary-layer flow accumulation near the suction surface and large radially inward flow at higher Mach numbers applies equally well to blade B as to blades A and C. However, within this broad framework there are notable differences between the results obtained for blade B compared with those for blades A and C. The differences in loss distribution were noted in the preceding section and in **RESULTS.** Also noted in **RESULTS** were the considerable differences in blade boundary-layer behavior between blades A and B as indicated by smoke flow tests (fig. 20). These differences are correlated with differences in blade velocity profiles in a later section.

COMPARISON OF DISCHARGE-ANGLE DISTRIBUTIONS OF BLADES A, B, AND C

For all three blades at the lower Mach numbers, the gradients of deviation of the discharge angles from design are quite small over most of the flow passage (figs. 11 (a), (c), (e), and 12 (b)). Furthermore, the circumferential mass-averaged flow angles (fig. 12 (b)) are close to the design angles except near the shrouds.

For the higher Mach numbers (figs. 11 (b), (d), (f), and 12 (c)), however, discharge-angle gradients distributed in the mainstream are increased. This effect is expected if, as suggested previously, there is an increasing general flow disturbance throughout the entire passage with increasing Mach number. As noted in the **RESULTS** section, the decreases in mass-averaged flow angles relative to design values were more pronounced near the inner shroud at the higher Mach numbers; whereas, near the outer shroud, the decreases were smaller for the higher Mach numbers. This is attributed to a combination of Prandtl-Meyer type expansion off the blade trailing edge (amounting to 5° at a Mach number of 1.25) and increased accumulation of low-momentum fluid near the inner shroud, which effectively blocked the flow and induced an increase in axial velocities in the immediate vicinity. Underturning and overturning of this magnitude result in rotor blade angles of attack that would cause a noticeable deterioration in performance. In this connection, it is noted that for blade C a nozzle discharge-angle variation of 13.6° near the inner shroud led to a variation in rotor blade angle of attack of 16.9° and a resulting loss of 1.5 percent of energy based on tangential component of velocity.

Large angle gradients were found in the shroud boundary layers, also, where overturning appears because of cross-channel secondary flows.

CORRELATION OF SECONDARY-FLOW PATTERNS WITH VELOCITY PROFILE OF BLADES A, B, AND C

Results obtained from the investigation of the three turbine nozzle blade types show how the different accumulations of loss, the different wake phenomena, and the different visual indications of secondary flow may possibly be correlated with each other and with the blade shapes and velocity profiles. For example, in figure 8 (c) the presence of a sizable loss core (suggestive of a flow vortex) is noted for the lower Mach number near the outer shroud downstream of nozzle blade B. By comparison, figures 8 (a) and (e) present the loss contours for the lower Mach numbers for blades A and C, in which such large outer-shroud loss cores do not appear. It is clear that the secondary flows that result in two such different loss-distribution patterns must themselves be considerably different. The reasons for these differences are discussed qualitatively in this section.

The discussion falls into three main parts. First, suction-surface velocity profiles are discussed and differences are noted in the boundary layer near the tip of blade B as compared with the other blade types. Then, the probable effects of these boundary-layer differences upon the behavior of the cross-channel secondary flows at the outer shrouds are considered. Finally, these considerations are shown to account for the differences in extent and magnitude of the wake losses measured behind the different kinds of blades and to provide an insight into the physical significance of such wake measurements.

Velocity profiles.—Suction-surface velocity profiles are plotted together for the three blades for hub, mean, and tip sections in figures 2 (a), (b), and (c), respectively. Mean-section blade shapes are also shown in figure 2 (b). The profiles were computed in each case for design (subsonic) Mach number. At other Mach numbers (at least in subsonic cases), velocity maximums and minimums might be expected to appear in similar locations.

For blades A and C, the profile plots show no sharp velocity peaks over the surface of any section. The blade B profile at the hub section, while not so smooth as the profiles of blades A and C, has only one maximum and might be expected to produce a fairly smooth flow. However, at the mean and particularly at the tip sections, blade B has profiles with two and three maximums, respectively, and each peak indicates a sudden change in velocity at one point. This nonuniformity may be actually greater than indicated, because the calculation methods based on differencing procedures and on representation of flow functions at a fixed number of points have a tendency to smooth the curves and thereby to reduce the magnitude of all computed velocity peaks. Such irregular profiles might reasonably be expected to cause a difference in boundary-layer behavior between blade B and the other two blades by causing flow separation or unusual boundary-layer growth on blade B.

Boundary layers.—The effects of blade shape and velocity profile on blade-surface boundary layer as described were shown visually by the smoke-injection studies. Figures 20 (a) and (b) for blade B indicate the presence of a large separated region on the suction surface of the blade where the tip-section velocity profile could be expected to affect the boundary layer. Apparently, the flow path followed by the smoke and accompanying low-momentum air did not actually reach the inner shroud in the vicinity of the trailing edge.

For blade A, having a smooth velocity profile, figure 20 (c) shows flow behavior indicating that the boundary layer on the blade suction surface was thinner than for blade B and was not separated.

Vortex formation.—The difference between blade suction-surface boundary layers previously indicated may be a basis for the difference between the larger outer-shroud loss region for blade B and the much smaller outer-shroud loss regions for the other two blades. For blade B, the separated flow near the outer shroud provided the condition required for formation of an appreciable vortex. That is, the outer-shroud boundary-layer air flowing into such a region might, and for blade B apparently did, roll up into the passage vortex type of flow described in reference 5. Once formed, the vortex resisted turning (ref. 5), tended to maintain its direction of flow, and passed into the wake near the outer shroud, where measurements showed the presence of a sizable loss core.

At the higher Mach number for blade B, the additional radial flow path provided by the thickened boundary layer on the blade suction surface due to shock formation in the passage serves to drain off more of the low-momentum fluid toward the inner shroud. This action effectively reduces the magnitude of the roll-up into a passage vortex.

No evidence of appreciable passage vortex formation near the outer shroud was observed for blades A and C, for which the blade boundary layers are thinner, as has been pointed out. The greatest portion of the low-momentum fluid originating along the outer shroud was swept radially inward into the wake and, therefore, was a contributing factor for the increased wake losses as compared with blade B. Also, for blades A and C, the part of the low-momentum fluid reaching the inner shroud contributes to the greater size of the inner-shroud loss region compared with that of the outer shroud.

Thus, the results suggest that passage vortex formation of measurable magnitude may not take place under all secondary-flow conditions, but only in those cases where blade shape and velocity profiles are such as to cause development of boundary-layer separation and stagnation regions extensive enough for the purpose.

Wake losses.—The phenomena described indicate an inward radial transfer of a smaller fraction of low-momentum fluid from the outer to the inner shroud for blade B than for the other blades. Thus, a smaller amount of low-momentum fluid from the outer shroud was found in the wake for this blade than for the others, as shown on the contour plots in figure 8. The magnitude and extent of wake loss behind a blade may, in some measure, be an indication of the radial flow taking place at the trailing edge or on the blade suction surface. Substantiating evidence is also indicated by the results of the study on blade C at the higher Mach number (figs. 8 (f) and 9 (b)), in which a flow fence was used to interrupt these radial flows. With the radial flow from the upper half of blade C interrupted at midspan, the loss measured in the wake from the lower half of the blade was reduced considerably.

At the lower Mach number, the loss accumulation for blade B near the inner shroud has roughly the same magnitude as for the other two blades. However, for blade B, with little radial flow, the greatest percentage of this loss must originate from the inner-shroud boundary layer. For the other blades, the measured inner-shroud loss region is a combination of inner-shroud loss and loss transferred radially in the wakes from the outer shroud. Barring radial flow, therefore, blades A and C would have smaller inner-shroud loss regions to compare with that of blade B.

Circulation.—The differences between the types of spanwise circulation distribution for the three blades were small. Furthermore, the total variations in circulation over the major portions of the blade spans are small compared with the changes in circulation in the blade-end boundary-layer regions. These circumstances make it difficult to judge, from the investigations of these blades, how spanwise variation in circulation affects secondary-flow patterns and loss distribution.

SUMMARY OF RESULTS AND CONCLUSIONS

The following results and conclusions were obtained from a study of secondary flows and loss accumulations in annular cascades of turbine nozzle blades of three different designs:

1. Two blade configurations (constant-discharge-angle blade A and vortex blade C, both with smooth suction-surface velocity profiles) showed the same secondary-flow patterns, namely, a cross-passage boundary-layer flow on the shrouds from pressure surfaces to suction surfaces and radial flow inward along the trailing edges of the blades. In addition, at supersonic conditions, radial flow took place inward along the suction surface through a strip of the boundary layer that had been thickened by shock interaction. These effects result in a pronounced accumulation of low-momentum air near the inner shroud and a greatly reduced outer-shroud loss region. At one flow condition (hub Mach number, 1.46), the radial flows in the blade C wake and the thickened boundary layer on the suction surface accounted for approximately 65 percent of the loss core, about 35 percent resulting from flow in the blade wake, and about 30 percent from flow in the thickened boundary layer.

2. For these two blade configurations (A and C), measured loss magnitudes and distributions were approximately the same, and no extreme discharge-angle gradients were encountered in the measuring plane.

3. The over-all integrated blade efficiencies were 0.99 and 0.98 in order of increasing Mach number for blade C. These efficiencies are not a good index of blade performance, because, while the energy loss involved in secondary flow is not large, the accumulation of large loss cores near the inner shroud where the diffusion is the greatest results in flow blockage there. This blockage gives rise to large flow-angle deviations, which, in turn, trigger additional losses in downstream blade rows.

4. Secondary flows can be intercepted by simple barriers in the flow paths of the low-momentum fluid. Thus, the degree of underturning at the inner wall, caused by blockage resulting from the loss accumulation by the secondary flow, can be reduced.

5. Comparison of the two sets of blades having smooth velocity profiles (A and C) with a set (constant discharge angle) having irregular suction-surface velocity profiles (B) shows that losses in general were greater and more concentrated for the blades with poorer velocity profiles. For this blade configuration (B), a passage vortex was apparently formed that carried a large loss region downstream near the outer shroud. At the higher Mach number, this blade configuration showed indications of radial flow of large amounts of low-mometum fluid to form a large loss region near the inner shroud, accompanied by severe discharge-angle gradients.

6. The blade flow conditions that contribute to the formation of a passage vortex near the outer shroud appear to be blade boundary-layer thickening and separation, which are produced by irregular suction-surface velocity profiles.

7. Magnitude and extent of blade wakes is dependent upon secondary-flow conditions. The loss measured in the wake at any radial position is a combination of profile losses and low-momentum air flowing radially inward from points nearer the outer shroud. Thus, the blade configuration having little tendency for passage vortex formation has, as a result, more pronounced wakes.

8. Because of the similarity between loss magnitudes and distributions and between secondary flows for the two blade configurations having smooth velocity profiles (constant-discharge-angle blade A and vortex blade C), it appears that on the basis of secondary flow alone there is no reason to choose one of the two blade types rather than the other. The difference in the variation of design spanwise circulation for the two is small, and the large boundary-layer and secondary-flow effects seem to mask any effects that may exist because of the main-span circulation differences.

9. In the region of high velocity gradients (particularly in the loss region near the inner shroud and for the higher Mach number), the accuracy of measurements of pressure and flow angle may be limited, and the interpretation of these measurements should be made with care.

LEWIS FLIGHT PROPULSION LABORATORY
NATIONAL ADVISORY COMMITTEE FOR AERONAUTICS
CLEVELAND, OHIO, *April 30, 1953*

APPENDIX

APPLICATION OF HOT-WIRE-ANEMOMETER PROBE

PARALLEL-WIRE PROBE

The hot-wire probe for measuring flow angles in the main part of the air stream consisted of two wires (of 80 percent platinum and 20 percent iridium) mounted in spatial and electrical parallelism. The wires were supported on two Inconel prongs with their lengths perpendicular to the air stream and parallel to the axis of the probe and rotation. The alinement of the wires with the air stream was detected electrically by observing the maximum in potential drop when the downstream wire temperature reached a peak as a result of receiving heat by convection through the wake from the upstream wire.

The electrical equipment used for the discharge-flow-angle investigation with this hot-wire-anemometer probe consisted essentially of a bridge circuit, a direct-current power supply with which the current could be easily adjusted over a continuous range, a direct-current voltage amplifier, and a voltmeter for indication of the bridge output voltage. A probe actuator with appropriate switching arrangement was used to control the angular orientation of the hot-wire array with the air flow. The circuit employed in obtaining angle data, as well as the theory and procedure, is discussed in reference 3.

A compromise among wire sensitivity, effects of radial angle gradients, and wire life determined the size of the wires used for the investigation. A satisfactory wire life in the filtered-air supply limited the wire diameter to a minimum of 0.0009 inch. The wire length was kept small (0.045 in. or less) to reduce the effects of radial angle gradients. In spite of the small length, the extremely small wire diameter as compared with wire length resulted in a large wire length-to-diameter ratio and helped to increase the angle sensitivity and to minimize the effects of the supports on the wire operation. The wire operating temperature of approximately 250° C and wire spacing of 0.005 inch gave good sensitivity.

Wire damage from collision by dirt particles in the air supply either made the probe inoperative or changed the original wire orientation, thereby changing the reference-angle calibration. Frequent checking of a previous data point was therefore essential to prevent data errors resulting from change in wire orientation due to wire damage.

When the pair of heated wires was alined with the air stream, notation of the reversals of the change of bridge output voltage was made visually. Several reversals were usually made to obtain an accurate angle value. The variation in a set of readings was on the order of $\pm 0.5°$ for most series.

V-WIRE PROBE

The probe consisting of a radially mounted parallel pair of wires was thought to be unsuitable for boundary-layer measurements near the inner shroud, because large nonuniform radial angle gradients exist in this boundary layer and also because the wire length limits the minimum radial distance between survey point and inner shroud to about 0.035 inch. Therefore, a V-wire probe was constructed with wires of the same material as the parallel-wire probe mounted in a plane perpendicular to the probe axis and parallel to the shroud surface in the vicinity of the measuring point. In operation, a reproducible orientation of the wires with respect to the air-flow direction was obtained by rotating them about the probe axis until the resistance ratio of the two wires with convective heat loss due to the air stream was the same as their resistance ratio with no convective heat loss. The procedure involved obtaining an angle reading for this rotative position at a point where the flow direction was known and comparing angle readings at other points with this known angle.

The electrical equipment used with the V-wire probe was essentially the same as with the parallel-wire probe, except that the two wires were balanced against each other rather than against a constant resistance. Also, a sensitive galvanometer was used as an indicating instrument instead of the amplifier-voltmeter combination required for the parallel wires.

As in the use of the parallel wires, frequent checking of a previous data point was necessary to detect wire damage immediately and thereby avoid data errors.

REFERENCES

1. Carter, A. D. S., and Cohen, Elizabeth M.: Preliminary Investigation into the Three-Dimensional Flow through a Cascade of Aerofoils. R. & M. No. 2339, British A. R. C., Feb. 1946.
2. Squire, H. B., and Winter, K. G.: The Secondary Flow in a Cascade of Airfoils in a Nonuniform Stream. Jour. Aero. Sci., vol. 18, no. 4, Apr. 1951, pp. 271–277.
3. Hawthorne, William R.: Secondary Circulation in Fluid Flow. Proc. Roy. Soc. (London), ser. A, vol. 206, no. A1086, May 7, 1951, pp. 374–387.
4. Kronauer, Richard E.: Secondary Flows in Fluid Dynamics. Pratt and Whitney Res. Rep. No. 132, Gordon McKay Lab., Harvard Univ., Apr. 1951.
5. Herzig, Howard Z., Hansen, Arthur G., and Costello, George R.: A Visualization Study of Secondary Flows in Cascades. NACA Rep. 1163, 1954. (Supersedes NACA TN 2947.)
6. Huppert, M. C., and MacGregor, Charles: Comparison Between Predicted and Observed Performance of Gas-Turbine Stator Blade Designed for Free-Vortex Flow. NACA TN 1810, 1949.
7. Lowell, Herman H.: Design and Applications of Hot-Wire Anemometers for Steady-State Measurements at Transonic and Supersonic Airspeeds. NACA TN 2117, 1950.
8. Barry, F. W., Shapiro, A. H., and Neumann, E. P.: The Interaction of Shock Waves with Boundary Layers on a Flat Surface. Jour. Aero. Sci., vol. 18, no. 4, Apr. 1951, pp. 229–238.
9. Scarborough, James B.: Numerical Mathematical Analysis. The Johns Hopkins Press (Baltimore), 2d ed., 1950.
10. Zucrow, Maurice Joseph: Principles of Jet Propulsion and Gas Turbines. John Wiley & Sons, Inc., 1948.
11. Kochendorfer, Fred D., and Nettles, J. Cary: An Analytical Method of Estimating Turbine Performance. NACA Rep. 930, 1949. (Supersedes NACA RM E8I16.)
12. Goldstein, Arthur W.: Analysis of Performance of a Jet Engine from Characteristics of Components. I–Aerodynamic and Matching Characteristics of Turbine Component Determined with Cold Air. NACA Rep. 878, 1947. (Supersedes NACA TN 1459.)

TABLE I.—NOZZLE BLADE PROFILE COORDINATES FOR BLADE A

(a) Profile coordinates.

X, in.	Section					
	Root		Mean		Tip	
	Radius, in.					
	5.939		7.003		8.122	
	Y_L, in.	Y_U, in.	Y_L, in.	Y_U, in.	Y_L, in.	Y_U, in.
0	0.036	0.036	0.046	0.046	0.050	0.050
.100	.025	.183	.022	.197	.021	.213
.200	.064	.232	.067	.258	.069	.280
.300	.090	.250	.099	.285	.104	.318
.400	.105	.246	.119	.292	.131	.131
.500	.110	.229	.131	.283	.149	.335
.600	.105	.206	.133	.266	.158	.324
.700	.093	.177	.126	.242	.157	.304
.800	.077	.146	.115	.213	.151	.280
.900	.058	.115	.101	.185	.140	.254
1.000	.036	.084	.083	.156	.127	.227
1.100	.013	.053	.064	.127	.111	.198
1.173	.017	.017	-----	-----	-----	-----
1.200	-----	-----	.042	.098	.093	.170
1.300	-----	-----	.020	.069	.073	.142
1.409	-----	-----	.022	.022	-----	-----
1.500	-----	-----	-----	-----	.029	.084
1.600	-----	-----	-----	-----	.004	.055
1.642	-----	-----	-----	-----	.025	.025

(b) Stacking coordinates.

X, in.	Section		
	Root	Mean	Tip
	Y, in.	Y, in.	Y, in.
0.071	0.073	-----	-----
.100	-----	0.102	-----
.128	-----	-----	0.131
.385	.175	-----	-----
.414	-----	.205	-----
.442	-----	-----	.234
.675	.140	-----	-----
.705	-----	.170	-----
.733	-----	-----	.199

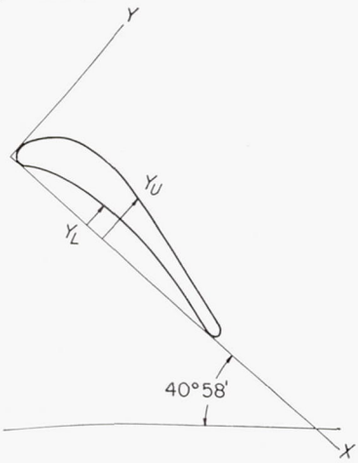

TABLE II.—NOZZLE BLADE PROFILE COORDINATES FOR BLADE B

(a) Profile coordinates.

X, in.	Section					
	Root		Mean		Tip	
	Radius, in.					
	5.939		7.003		8.122	
	Y_L, in.	Y_U, in.	Y_L, in.	Y_U, in.	Y_L, in.	Y_U, in.
0	0.083	0.083	0.099	0.099	0.117	0.117
.125	.001	.248	.004	.279	.000	.304
.225	.052	.286	.045	.327	.037	.361
.325	.079	.297	.080	.347	.076	.393
.425	.096	.291	.102	.351	.106	.406
.525	.104	.275	.115	.342	.124	.403
.625	.105	.249	.121	.325	.133	.392
.725	.099	.216	.121	.300	.138	.376
.825	.085	.177	.114	.268	.138	.351
.925	.063	.133	.101	.231	.131	.321
1.025	.035	.086	.081	.189	.118	.286
1.125	.005	.038	.059	.144	.100	.247
1.157	.013	.013	-----	-----	-----	-----
1.225	-----	-----	.035	.100	.081	.204
1.325	-----	-----	.009	.052	.058	.158
1.373	-----	-----	.017	.017	-----	-----
1.425	-----	-----	-----	-----	.035	.114
1.525	-----	-----	-----	-----	.011	.065
1.592	-----	-----	-----	-----	.020	.020

(b) Stacking coordinates.

X, in.	Section		
	Root	Mean	Tip
	Y, in.	Y, in.	Y, in.
0.206	0.167	-----	-----
.325	-----	0.210	-----
.385	.175	-----	-----
.446	-----	-----	0.252
.505	-----	.218	-----
.625	-----	-----	.260
.706	.143	-----	-----
.826	-----	.180	-----
.946	-----	-----	.208

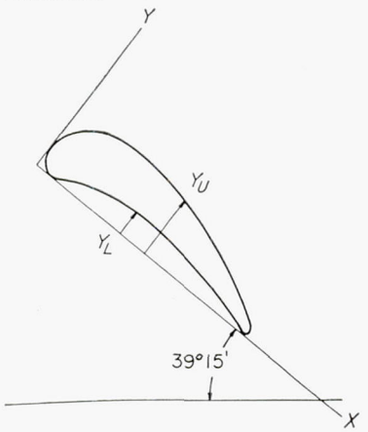

TABLE III.—NOZZLE BLADE PROFILE COORDINATES FOR BLADE C

(a) Profile coordinates.

X, in.	Section					
	Root		Mean		Tip	
	Radius, in.					
	5.939		7.003		8.122	
	Y_L, in.	Y_U, in.	Y_L, in.	Y_U, in.	Y_L, in.	Y_U, in.
0	0.038	0.038	0.059	0.059	0.082	0.082
.100	.032	.183	.016	.216	.002	.238
.200	.089	.237	.071	.267	.047	.292
.300	.130	.264	.109	.292	.087	.320
.400	.153	.268	.134	.300	.117	.311
.500	.160	.257	.147	.293	.138	.329
.600	.154	.234	.152	.279	.151	.319
.700	.139	.206	.149	.259	.159	.303
.800	.116	.174	.140	.235	.159	.283
.900	.087	.138	.124	.207	.153	.260
1.000	.055	.099	.104	.177	.142	.234
1.100	.020	.058	.082	.145	.127	.207
1.172	.017	.017	-----	-----	-----	-----
1.200	-----	-----	.056	.112	.109	.180
1.300	-----	-----	.030	.079	.089	.152
1.400	-----	-----	.001	.044	.067	.123
1.428	-----	-----	.020	.020	-----	-----
1.500	-----	-----	-----	-----	.043	.095
1.600	-----	-----	-----	-----	.019	.067
1.697	-----	-----	-----	-----	.022	.022

(b) Stacking coordinates.

X, in.	Section		
	Root	Mean	Tip
	Y, in.	Y, in.	Y, in.
0.065	0.074	-----	-----
.094	-----	0.102	-----
.122	-----	-----	0.130
.638	.192	-----	-----
.667	-----	.220	-----
.695	-----	-----	.248

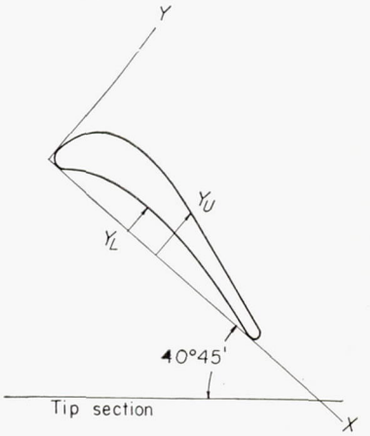

U. S. GOVERNMENT PRINTING OFFICE: 1954